

A past and present perspective on the European summer vapour pressure deficit

Viorica Nagavciuc^{1,2 *†}, Simon L. L. Michel^{3†}, Daniel F. Balting^{1†}, Gerhard Helle⁴, Mandy Freund⁵,
5 Gerhard H. Schleser⁶, David N. Steger⁷, Gerrit Lohmann^{1,8} and Monica Ionita^{1,2,9}

¹Alfred-Wegener-Institute, Bremerhaven, 27570, Germany

²Faculty of Forestry, Ștefan cel Mare University, Suceava, 720229, Romania

³Institute for Marine and Atmospheric Research Utrecht (IMAU), Department of Physics, Utrecht University, Utrecht, Netherlands

10 ⁴German Research Centre for Geosciences, Potsdam, 14473, Germany

⁵Climate and Energy College, University of Melbourne, Melbourne, VIC 3010, Australia

⁶Institute of Bio- and Geosciences IBG-3, Forschungszentrum Jülich, Jülich 52428, Germany

⁷University of Basel, Department of Environmental Sciences, Basel, 4056, Switzerland

⁸Physics Department, University of Bremen, Bremen, 28359, Germany

15 ⁹Emil Racovita Institute of Speleology, Romanian Academy, Cluj-Napoca, 400006, Romania

*Correspondence to: Viorica Nagavciuc (viorica.nagavciuc@awi.de)

†Equally contributing co-authors

20 **Abstract.** The response of evapotranspiration to anthropogenic warming is of critical importance for the water and carbon cycle. Contradictory conclusions about evapotranspiration changes are caused primarily by their brevity in time and sparsity in space, as well as the strong influence of internal variability. Here, we present the first gridded reconstruction of the summer (June, July, and August) vapour pressure deficit (VPD) for the past four centuries at the European level. This gridded reconstruction is based on 26 European tree-ring oxygen isotope records and is obtained using a Random Forest approach.
25 According to validation scores obtained with the Nash–Sutcliffe model efficiency, our reconstruction is robust over large parts of Europe since 1600, in particular for westernmost and northernmost regions, where most tree ring records are located. Based on our reconstruction, we show that from the mid- 1700s, a trend towards higher summer VPD occurred in Central Europe and the Mediterranean region which is related to a simultaneous increase in temperature and decrease in precipitation. This increasing summer VPD trend continues throughout the observational period and in recent times. Moreover, our summer VPD
30 reconstruction helps to visualize the local and regional impacts of the current climate change as well as to minimize statistical uncertainties of historical VPD variability. Furthermore, the interdisciplinary use of the data should be emphasized, as summer VPD is a crucial parameter for many climatological feedback processes in the earth surface system. The reconstructed summer VPD gridded data, over the last 400 years, is available at the following link: <https://doi.org/10.5281/zenodo.5958836> (Balting, D. F. et al., 2022).

Evapotranspiration is a critical factor for understanding the links and feedback between atmospheric CO₂ and global climate (Good et al., 2015; IPCC, 2021b, 2021a). Within the terrestrial water fluxes, vegetation-produced transpiration represents the dominant factor (Good et al., 2015; IPCC, 2021b, 2021a). One key driver for such vegetation resources and dynamics is vapor pressure deficit (VPD), defined by the difference between the water vapor pressure at saturation and the actual water vapor pressure (Good et al., 2015; IPCC, 2021b, 2021a). The VPD represents the atmospheric evaporative demand which has an influence on the leaf-level transpiration of terrestrial vegetation and the corresponding stomatal conductance (Grossiord et al., 2020). With increasing VPD, the stomata closes to minimize water loss (Running, 1976) due to the high atmospheric evaporative demand. Consequently, a minimal stomata opening decreases stomatal conductance and photosynthetic activity (Fletcher et al., 2007). Extremely high VPD may even lead to reduced growth, a higher risk of carbon starvation, and hydraulic failure (Grossiord et al., 2020). In contrast, low VPD leads to reduced water transport into the leaves and thus a reduced supply of nutrients. Therefore, VPD is a crucial meteorological parameter with significant implications for agriculture, ecosystems, and various aspects of the environment (Novick et al., 2016), notably affecting plant growth and health: **VPD** affects transpiration rates, stomatal conductance, and overall water uptake by plants which overall controls the plant growth (Restaino et al., 2016); forest mortality (Williams et al., 2013), drought occurrence: high VPD values are associated with dry and arid conditions (Dai, 2013), crop production and quality: maintaining an optimal VPD range is crucial for maximizing photosynthesis, nutrient uptake, and ultimately, crop production, deviations from this range can lead to stress, reduced yields, and lower-quality produce (Zhao et al., 2017) and wildfire occurrence: high VPD values are associated with increasing risk of wildfires, understanding VPD can aid in wildfire prediction and management, helping to mitigate their destructive effects on both natural ecosystems and human settlements (Seager et al., 2015); ecosystem functioning: VPD affects the water balance in ecosystems, influencing the distribution and health of plant and animal species, changes in VPD due to climate variability can lead to shifts in vegetation patterns and affect biodiversity (Zhang et al., 2019), among others.

Since VPD is a function of temperature (Lawrence, 2005), the effects of climate change and the associated increase in the mean global temperature lead to positive trends in the regional and global VPD (Grossiord et al., 2020; IPCC, 2021b). For instance, studies have shown that the VPD has been increasing sharply at a global scale since the year 2000 (Simmons et al., 2010; Willett et al., 2014; Yuan et al., 2019). Spatially explicit VPD records derived from remote sensing data cover only the last ~50 years and vary in quality, so long-term perspectives of VPD variability are lacking. However, long-term perspectives can help to put recently observed trends of VPD in a long-term context relevant for estimating the significance and robustness of these changes both at local as well as at the continental scales. Furthermore, it is essential to investigate the independent physiological effects of VPD on large-scale vegetation dynamics, a topic which is far less explored (Grossiord et al., 2020). So far, the first local reconstruction studies have shown the potential for a long-term perspective on VPD (Liu et al., 2017; Roibu et al., 2022). Churakova Sidorova et al., (2020) have shown that the recent VPD increase does

not yet exceed the maximum values reconstructed during the Medieval Warm Anomaly in Siberia. Nevertheless, most studies lack a wider spatial perspective as they only reconstruct VPD time series for a single location. Therefore, it appears necessary for high resolution VPD reconstructions over extended spatial regions (e.g. the European region).

Tree-ring sequences are one of the most used proxy archives for paleoclimatic and environmental reconstructions because of their annual resolution, precise dating, and widespread spatial extent (Leonelli et al., 2017). Moreover, they allow us to create chronologies of thousands of years and give us the possibility to explore the climate through different tree ring-based climate-sensitive parameters, such as: tree-ring width, maximum density, and/or stable isotopes (Nagavciuc et al., 2022). Of all physical or chemical parameters to be measured of annual rings, the stable oxygen isotope ratio of tree-ring cellulose ($\delta^{18}\text{O}$) has the advantage that the isotopic fractions controlled by physiological processes are reasonably well understood and the statistical relationship with climatic and environmental quantities is rather robust (McCarroll and Loader, 2004; Siegwolf et al., 2022). Combining these advantages with the advantages of annual tree rings, stable oxygen isotopes in tree-ring cellulose may be one of the most valuable proxies for the paleoclimatic reconstructions. Nonetheless, there are still questions to be answered about the variability of $\delta^{18}\text{O}$ in the arboreal system (Gagen et al., 2022).

The $\delta^{18}\text{O}$ in tree-ring cellulose is mainly influenced *i*) by $\delta^{18}\text{O}$ signature of precipitation (through water uptake by the roots from the soil) (McCarroll and Loader, 2004; Siegwolf et al., 2022); *ii*) by biochemical fractionation including partial isotopic exchange of cellulose precursors with stem water during cellulose biosynthesis (Barbour, 2007; Roden et al., 2000; Saurer et al., 1997), which is considered to be largely constant at $27\pm 4\text{‰}$ (Sternberg and DeNiro, 1983); and most important *iii*) the evaporative ^{18}O enrichment of leaf or needle water via transpiration of water vapor to the atmosphere (Kahmen et al., 2011; Roden et al., 2000; Saurer et al., 1997). The transpiration process is controlled by leaf-to-air VPD modified by the aperture of stomata controlling the conductance for water vapor (Buckley, 2019; McCarroll and Loader, 2004). The $\delta^{18}\text{O}$ values of leaf water are typically enriched in ^{18}O compared to the plant's parent water because evaporative losses are greater for the lighter ^{16}O than for ^{18}O (Roden et al., 2000). However, $\delta^{18}\text{O}$ features the $\delta^{18}\text{O}$ signature of chloroplast water which is not in isotopic equilibrium with leaf water at the actual sites of transpiration (stomata), i.e. the higher the transpiration rates the lower is the rate of enrichment of the chloroplast water, so called Péclet effect (Barbour et al., 2004). To a good approximation, tree ring- $\delta^{18}\text{O}$ from European sites can be considered as a combined signal of the largely temperature-dependent $\delta^{18}\text{O}$ of the water source (precipitation, soil water) and the evaporative ^{18}O enrichment of leaf water controlled by leaf-to-air VPD, so that tree ring- $\delta^{18}\text{O}$ can be used as a proxy for variations in VPD (Ferrio and Voltas, 2005; Kahmen et al., 2011).

In order to have a long-term overview of the observed changes and trends in the regional and global VPD, one needs to look back in the past, by employing different proxy indicators (e.g. from tree rings). In this respect, the availability of the ISONET network (Balting et al., 2021; ISONET Project Members et al., 2023; Treydte et al., 2007a, 2007b) gave us the opportunity to develop the first VPD reconstruction at the European level, by using multiple stable oxygen isotope records derived from tree-rings. The reconstruction of our VPD dataset, which covers the last 400 years, has been obtained by applying a Random Forest (RF) regression method (Breiman, 2001). According to Yang et al., (2020), RF has become one

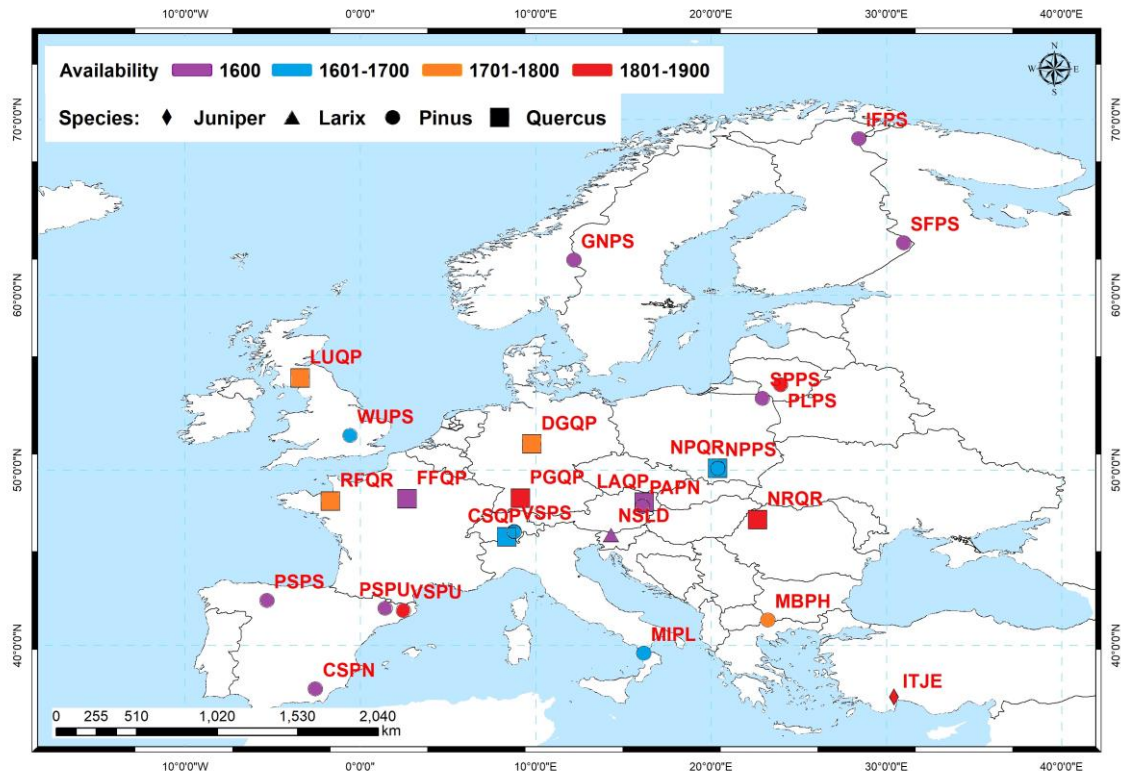
of the most successful machine learning algorithms for practical applications over the last two decades due to its proven accuracy, stability, speed of processing, and ease of use (Bair et al., 2018; Belgiu and Drăgu, 2016; Maxwell et al., 2018; Qu et al., 2019; Reichstein et al., 2019; Rodriguez-Galiano et al., 2012; Tyrallis et al., 2019). The term RF describes a non-linear and robust technique in which several decision trees are built and aggregated at the end to make predictions or perform reconstructions (Breiman, 2001). The RF approach is increasingly applied in climate and environmental sciences, and has been used for the prediction of snow depth (Yang et al., 2020), solar radiation (Prasad et al., 2019), daily ozone (Zhan et al., 2018), precipitation (Ali et al., 2020); as well as for reconstructions of last millennium North Atlantic Oscillation (Michel et al., 2020), Atlantic Multidecadal Variability (Michel et al., 2022), El Niño Southern Oscillation (Delcroix et al., 2022), streamflow since 1485 C.E. (Li et al., 2019) and vegetation cover during the mid-Holocene and the Last Glacial Maximum (Lindgren et al., 2021), as well as for tree growth response to earthquakes (Mohr et al., 2021). Although RF models have proved to be a useful method in geosciences, studies on the spatial-temporal reconstruction of climate variables based on $\delta^{18}\text{O}$ are relatively rare due to the low availability of $\delta^{18}\text{O}$ time series. Here, the RF model is used independently for the reconstruction of each grid point, meaning that we build several 1-dimensional climate time series reconstruction models where the respective weights of the $\delta^{18}\text{O}$ values of tree-ring cellulose varies for each grid point (see Methods). In this regards, recent studies reconstructing climate time series as here, showed that RF generally outperforms most commonly used variants of linear regression model (*e.g.*, principal component regression, partial least squares..., (Delcroix et al., 2022; Michel et al., 2020, 2022)).

The purpose of this study is to apply a RF approach (Breiman, 2001) for reconstructing the European summer (averaged for June-July-August) VPD for the first time, from a proxy network that is based on 26 series of tree-ring $\delta^{18}\text{O}$ and covers the period 1600-1994 (Balting et al., 2021; ISONET Project Members et al., 2023). The main aim is to present the summer VPD reconstruction dataset for the last 400 years over Europe and provide both a spatial as well as a temporal long-term perspective on the past summer VPD variability. The VPD reconstruction is analyzed subsequently from a spatio-temporal perspective for Northern Europe, Central Europe, and Mediterranean regions (Iturbide et al., 2020) as defined and used in the Sixth Assessment Report (AR6) of the IPCC (IPCC, 2021a). The data evaluation in this paper is structured as follows: in Section 2 we give a detailed description of the data and methods employed, while the main results are presented in Section 3: first, we present the sensitivity of $\delta^{18}\text{O}$ for VPD variability and the validations statistics for the reconstruction; second, we investigate the spatial variability of VPD in comparison with other studies and analyses for selected extreme years, for additional validation of our reconstructions. Statistical uncertainties are discussed in Section 4, while conclusions and outlooks are presented in Section 5. In this way, the past and present VPD conditions are presented and evaluated to assess the statistical significance of observed trends to understand VPD variability on a local, regional, and continental scale.

2. Data and Methods

2.1 The stable isotope network

To reconstruct the European summer VPD, we used 26 time series of stable oxygen isotopes in tree-ring cellulose ($\delta^{18}\text{O}$) (Figure 1, Table 1). From the 26 time series used in this study, 21 time series were obtained from the dataset generated by the EU project ISONET (EVK2-CT-2002-00147) (Balting et al., 2021; ISONET Project Members et al., 2023; Treydte et al., 2007a, 2007b). In addition to the ISONET dataset, we added five new $\delta^{18}\text{O}$ time series from Bulgaria, Turkey, southwestern Germany, Romania, and Slovenia (Balting et al., 2021; Hafner et al., 2014; Heinrich et al., 2013; Nagavciuc et al., 2019) (Figure 1).



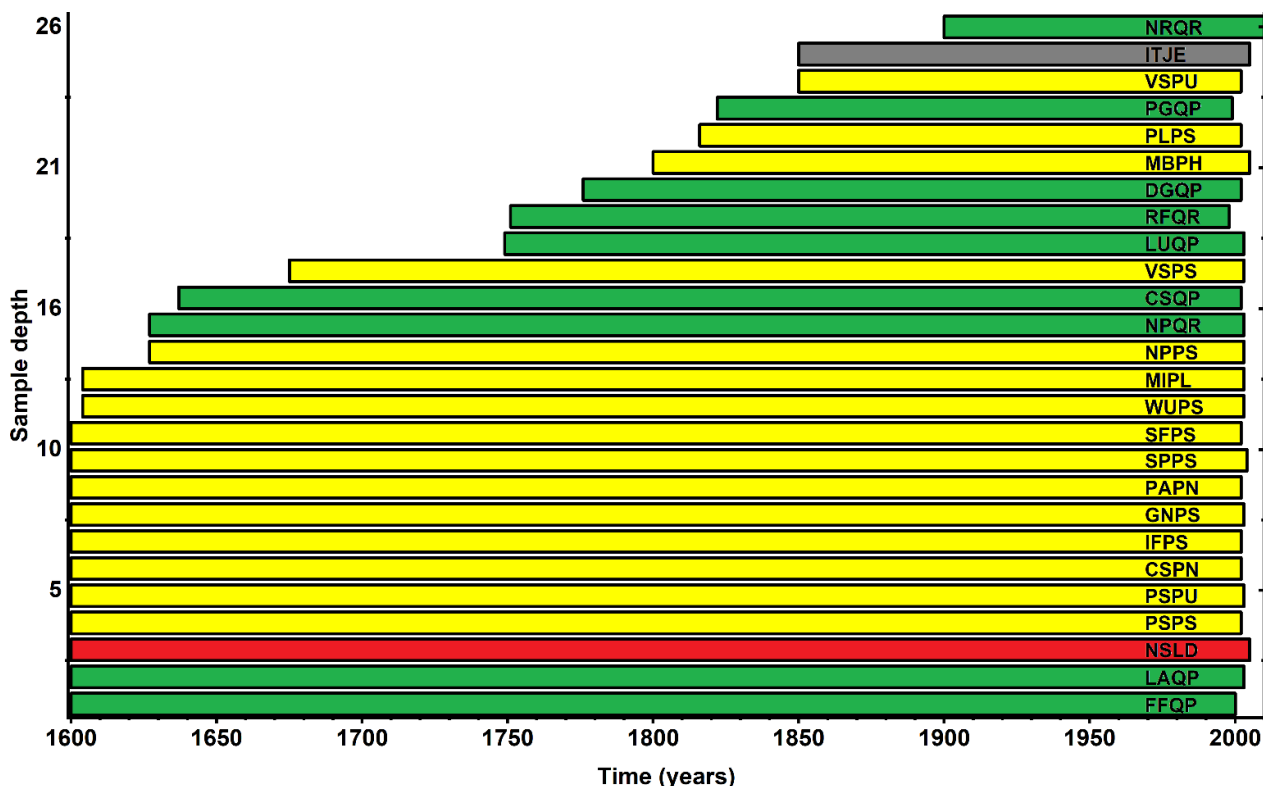
145

Figure 1: The site distribution of the $\delta^{18}\text{O}$ network composed of 21 ISONET and 5 additional data (see Table 1). Colors indicate the past temporal availability of each tree ring data: starts in 1600 or earlier (purple), starts between 1601 and 1700 (blue), starts between 1701 and 1800 (blue), starts between 1801 and 1900 (blue). Symbols indicate tree species used for each record: Juniper (diamond), Larix (triangle), Pinus (circle), Quercus (square).

150

The detailed measurement methodologies used within the ISONET project as well as for the other sites are described in the description file of the data set (ISONET Project Members et al., 2023) and, in more detail, in the previously published

papers (Boettger et al., 2007; Hafner et al., 2014; Heinrich et al., 2013; Nagavciuc et al., 2019; Treydte et al., 2007b, 2007a). At least four dominant trees were selected at each site and two increment cores were taken per tree for the ISONET project; 155 15 cores of five living trees were taken from the site in Turkey (Heinrich et al., 2013), 12 trees were sampled for the Slovenian time series (Hafner et al., 2014) and from nine trees, one core per tree was taken in Romania (Nagavciuc et al., 2019). A standard dendrochronological dating method was performed (Fritts, 1976), and subsequent individual growth rings were dissected from the cores. All tree rings from the same year were pooled for most sites prior to cellulose extraction for the ISONET sites (Treydte et al., 2007b, 2007a) as well as for the Romanian site (Nagavciuc et al., 2019). The dissected tree rings 160 from the Slovenian and Turkish sites were measured individually and not pooled (Hafner et al., 2014; Heinrich et al., 2013). For oak, only the latewood was used for the analyses. This approach was assumed to use predominantly climate signals from the current year, as the earlywood of oaks can contain climate information from the previous year (Davies and Loader, 2020; González-González et al., 2015). All $\delta^{18}\text{O}$ time series were measured according to standard methodology and the inter-lab differences are assumed negligible for future analysis. The results are expressed using the conventional δ (delta) notation, in 165 per mil (‰) relative to the Vienna Standard Mean Ocean Water (VSMOW) (Craig, 1957).



170 **Figure 2:** The number of available $\delta^{18}\text{O}$ time series within the network composed of 21 ISONET and 5 additional data (see Table 1). The *Quercus* sites are represented with green color, *Pinus* sites with yellow, *Larix* with red, and *Juniperus* with grey. For site codes please see table 1.

The isotope network presented here consists of nine deciduous tree sites (*Quercus*) and 17 conifer sites (*Pinus*, *Juniper*, *Larix*; see Table 1). The sample sites are well distributed over Europe (Figure 1). The elevation of the locations varies from 10 m a.s.l. (Woburn, UK) to 2.120 m a.s.l. (Pedraforca, Spain). The longest chronologies cover a period from 1600 to 2005. The highest data density (i.e., 26 time series) is available for the period 1900-1994 (Figure 2). For several sites or regional groups of sites from the ISONET datasets, the data is published within individual studies (Andreu-Hayles et al., 2017; Etien et al., 2008; Haupt et al., 2011; Helama et al., 2014; Hiltunen et al., 2009; Labuhn et al., 2014, 2016; Rinne et al., 2013; Saurer et al., 2014, 2008, 2012; Vitas, 2008).

Table 1: Characteristics of each sample site used within our study. 21 of the 26 $\delta^{18}\text{O}$ records were obtained from the EU project ISONET and five additional sites from Bulgaria, Turkey, Southwest Germany, Romania, and Slovenia.

	Code	Location	Country	Species	First year	Last year	Lon.	Lat.	Altitude	Source
1	CSPN	Cazorla	Spain	<i>Pinus nigra</i>	1600	2002	-2.57°	37.53°	1820 m	ISONET
2	CSQP	Cavergno	Switzerland	<i>Quercus petraea</i>	1637	2002	8.36°	46.21°	900 m	ISONET
3	DGQP	Dransfeld	Germany	<i>Quercus petraea</i>	1776	2002	9.78°	51.50°	320 m	ISONET
4	FFQP	Fontainebleau	France	<i>Quercus petraea</i>	1600	2000	2.67°	48.38°	100 m	ISONET
5	GNPS	Gutuli	Norway	<i>Pinus sylvestris</i>	1600	2003	12.18°	62.00°	800 m	ISONET
6	IFPS	Inari	Finland	<i>Pinus sylvestris</i>	1600	2002	28.42°	68.93°	150 m	ISONET
7	ITJE	Isibeli	Turkey	<i>Juniper excelsa</i>	1850	2005	30.45°	37.06°	1800 m	(Heinrich et al., 2013)
8	LAQP	Lainzer Tiergarten	Austria	<i>Quercus petraea</i>	1600	2003	16.20°	48.18°	300 m	ISONET
9	LUQP	Lochwood	United Kingdom	<i>Quercus petraea</i>	1749	2003	-3.43°	55.27°	175 m	ISONET
10	MIPL	Monte Pollino	Italy	<i>Pinus leucodermis</i>	1604	2003	16.16°	39.58°	1900 m	ISONET
11	MBPH	Mount Vichren	Bulgaria	<i>Pinus heldreichii</i>	1800	2005	23.24°	41.46°	1900 m	(Balting et al., 2021)

12	NSLD	Naklo	Slovenia	<i>Larix decidua</i>	1600	2005	14.30°	46.30°	440 m	(Hafner et al., 2014)
13	NPQR	Niepolomice	Poland	<i>Quercus robur</i>	1627	2003	20.38°	50.12°	190 m	ISONET
14	NPPS	Niepolomice	Poland	<i>Pinus sylvestris</i>	1627	2003	20.38°	50.12°	190 m	ISONET
15	NRQR	Nusfalau	Romania	<i>Quercus robur</i>	1900	2016	22.66°	47.19°	270 m	(Nagavciuc et al., 2019)
16	PLPS	Panemunės	Lithuania	<i>Pinus sylvestris</i>	1816	2002	23.97°	54.88°	45 m	ISONET
17	PSPU	Pedraforca	Spain	<i>Pinus uncinata</i>	1600	2003	1.42°	42.13°	2120 m	ISONET
18	PSPS	Pinar de Lillo	Spain	<i>Pinus sylvestris</i>	1600	2002	-5.34°	42.57°	1600 m	ISONET
19	PGQP	Plieningen	Germany	<i>Quercus petraea</i>	1822	1999	9.13°	48.42°	340 m	(Balting et al., 2021)
21	PAPN	Poellau	Austria	<i>Pinus nigra</i>	1600	2002	16.06°	47.95°	500 m	ISONET
20	RFQR	Rennes	France	<i>Quercus robur</i>	1751	1998	-1.7°	48.25°	100 m	ISONET
22	SFPS	Sivakkovaara	Finland	<i>Pinus sylvestris</i>	1600	2002	30.98°	62.98°	200 m	ISONET
23	SPPS	Suwalki	Poland	<i>Pinus sylvestris</i>	1600	2004	22.93°	54.10°	160 m	ISONET
24	VSPS	Vigera	Switzerland	<i>Pinus sylvestris</i>	1675	2003	8.77°	46.50°	1400 m	ISONET
25	VSPU	Vinuesa	Spain	<i>Pinus uncinata</i>	1850	2002	2.45°	42.00°	720 m	ISONET
26	WUPS	Woburn	United Kingdom	<i>Pinus sylvestris</i>	1604	2003	-0.59°	51.98°	10 m	ISONET

2.2 Climate data

185 Mean air temperature (°C) and relative humidity (%) from the near-surface (i.e., 2m above ground level) were derived from the 20th Century Reanalysis Project (20CR) version V3 (Slivinski et al., 2019) at a monthly resolution, to build the statistical model for VPD reconstruction. The 20CR reanalysis has a temporal resolution of three hours, 28 different pressure levels, and a resolution of 1° x 1°. We use the ensemble mean derived from an 80-member ensemble. The climate variables are available for the period from 1836 to 2015 and they are provided by NOAA/OAR/ESRL PSL, Boulder, Colorado, USA (https://psl.noaa.gov/data/gridded/data.20thC_ReanV3.html).

190

2.3 VPD computation and further pre-processing

The monthly VPD values were calculated based on the equation presented by Barkhordarian et al., (2019) by using the near-surface air temperature (e.g., 2m above the ground) (T) and the dew point temperature (T_d), both in °C. Since dew point

temperature is not available for each grid point of the datasets, we have used T and relative humidity (RH, %) to compute T_d as follows:

$$(1) \quad T_d = \frac{a_1 \left(\ln\left(\frac{RH}{100}\right) + \frac{Ta_2}{T+a_1} \right)}{a_2 - \left(\ln\left(\frac{RH}{100}\right) + \frac{Ta_2}{T+a_1} \right)}$$

Where a_1 and a_2 are defined as $a_1 = 243.04$ and $a_2 = 17.625$. This computation is reliable and is notably used in many climate models (Barkhordarian et al., 2019). We utilize the Clausius–Clapeyron relation, by applying a term for the saturation vapor content of the air and a term for the actual vapor pressure to calculate VPD as follows in the equation (2) (Barkhordarian et al., 2019; Behrangi et al., 2016; Marengo et al., 2008; Seager et al., 2015):

$$(2) \quad VPD = c_1 \times e^{\left(\frac{c_2 * T}{c_3 + T}\right)} - c_1 \times e^{\left(\frac{c_2 * T_d}{c_3 + T_d}\right)}$$

where $c_1 = 0.611$ kPa, $c_2 = 17.5$, $c_3 = 240.978$ °C, and VPD (kPa) (see (WMO, 2018) for further information). We calculated these quantities for monthly reanalysis averages and computed seasonal VPD average for summer (JJA June to August) on which we will focus our analyses in the following.

Here, we use the 20CR reanalysis as it spans a large enough time frame to calibrate statistical reconstruction models, which is at the expense of increased data uncertainties. To ensure that values from 20CR are in line with other historical VPD estimates, we also computed VPD for the ERA5 reanalysis dataset (Hersbach et al., 2020) over the European area (10°W-40°E, 35°N-75°N) where we find good agreement between both datasets (Supplement Figure S1).

2.4 Application of Random Forest

The VPD data derived from 20CRV3 ((Slivinski et al., 2019), section 2.3) and the $\delta^{18}\text{O}$ network data were used as input. There is a small number of missing data in the $\delta^{18}\text{O}$ time series (0.38% entries in total) which are infilled using an iterative Principal Component Analysis approach following Josse and Husson, (2016).

To reconstruct spatially the European summer VPD for the last 400 years we have used the Random Forest (RF) method (see Supplement Section 1 and Figure S2 for details) (Breiman, 2001). The RF is an ensemble bootstrapping method consisting of aggregating several predictions given by simple, and generally poorly efficient, non-linear regression trees (Breiman, 2001). Regression trees consist of a recursive convex optimization. First, the predictor ($\delta^{18}\text{O}$ time series here) which best splits the initial summer VPD values in time into two groups (leaves) where their Euclidean distances with group centers are minimized. This is recursively applied where the specific group giving the best split is also considered in the minimization (on top of the $\delta^{18}\text{O}$ time series and its values best splitting summer VPD data). The algorithm stops when one group is composed of a threshold number of VPD values. In the case of using regression trees within a RF, this threshold is recommended to be set to 5 which we will do here for all RF models, as its optimization is costly and generally not worth the computation (Breiman, 2001). Regression trees generally overfit the data they are trained with since removing one single predictor (for instance the

$\delta^{18}\text{O}$ time series used at the first split of the tree) can result in drastically different modeled data (Breiman, 2001). This is the reason why RF was developed: it consists in constructing several regression trees, each based on a randomly drawn sample of the initial set of $\delta^{18}\text{O}$ time series. The number of trees was shown to give converging predictions for a wide variety of datasets when set to 256 or higher (Oshiro et al., 2012). Hence, we here used a number of 256 trees for all RF models we have computed. Finally, the number of random predictors (i.e., $\delta^{18}\text{O}$ time series) selected is tuned using a 10-fold cross validation (Michel et al., 2020, 2022) for all RF models of the study in a possible range extending from one to the number of initially selected $\delta^{18}\text{O}$ time series (see next paragraph). See supplementary section 1 for further details. Once a RF model is trained and tuned from cross validation, a reconstruction is obtained by browsing all trees from the training using the values of $\delta^{18}\text{O}$ time series in the past. The reconstructed summer VPD value is obtained as the average of values.

235

2.5 General procedure of the European VPD reconstruction

The RF algorithm as used here is not directly adapted for spatial reconstruction. We thus computed several RF models tuned with cross-validation, each specifically computed for the reconstruction of a single grid point. For climate time series reconstruction as performed here, RF was shown to most generally overclass several linear regression methods, including principal component regression that has been extensively used in the climate reconstruction literature (e.g., (Ortega et al., 2015; Wang et al., 2017)Ortega et al., 2015, Wang et al., 2017). For each grid point of the observations, sensitivity tests are performed prior to the reconstruction, where only $\delta^{18}\text{O}$ data significantly correlated at the 95% confidence level with the observed VPD are considered. This makes unique the reconstruction of each grid point from the summer VPD dataset as only relevant $\delta^{18}\text{O}$ time series are selected for each. These tests are carried out with a correction of the degrees of freedom using first order autocorrelation coefficients estimated from both timeseries as in Michel et al., (2020).

In our study, we focus on the continental area of the European region (9.5°W to 39.5°E and 35.5°N to 74.5°N). The learning is set from 1900 to 1994 which constitutes the longest period covered by all tree ring data from Table 1 starting from 1900 (Figure 2). Because $\delta^{18}\text{O}$ time series cover different periods in the past, we use a nesting approach to produce the reconstruction. Starting from the longest time frame of reconstruction (i.e., 1600-1994), a new gridded reconstruction is computed as a new $\delta^{18}\text{O}$ time series becomes available (see Table 1). At the end of the calculations, all imbricated time series for a given grid point are put one after the other to obtain the final reconstruction (Michel et al., 2022), which is done for all cells from the grid.

Each of the reconstruction for each grid point and nested time frame is evaluated by splitting up the data 30 times through time into training and testing samples, of 80% and 20% of the size of the initial learning period (i.e., 1900-1994), respectively. For each training sample, a RF model is built and tuned and a reconstruction of summer VPD for the testing period is obtained using corresponding values from $\delta^{18}\text{O}$ time series only. The evaluation over testing samples is made using the Coefficient of Efficiency score (S_{CE} , (Nash and Sutcliffe, 1970)). This score is defined from $-\infty$ to 1, where positive values indicate better reconstruction skill than what the empirical average of the training set would give. The reconstruction for a grid point over a given time frame of the nested reconstruction is thus considered robust and reliable only if the average

260 of the 30 $S_{\{CE\}}$ is significantly positive at the 95% confidence level through the sample, based on a one-tailed Student t-
test. Hence, our final reconstruction extending back to 1600 is composed of gaps in space and time, where filled data are only
those where robust reconstruction skills as described here were found. Once the RF model is evaluated through the 30
training/testing splits, a final reconstruction is computed as the median of the 30 individual reconstructions obtained from
training/testing splits. Therefore, statistical uncertainties of the gridded reconstruction are provided as the 10%-90% range of
265 these 30 individual reconstructions.

In addition, standard errors are computed from reconstructed time series with respect to summer VPD observations
over the period 1900-1994. For each grid point and each time frame of the nested reconstruction, we computed the uncertainties
as an envelope of twice the standard errors on each side of the reconstruction as in, e.g., (Ortega et al., 2015).

270 **2.6 Reconstruction analyses**

In order to further test the feasibility of our VPD reconstruction, in the final step of the analysis we compare the regional
averages and running averages (30 years) of the reconstructed VPD with temperature (Luterbacher et al., 2004), precipitation
(Pauling et al., 2006) and Palmer Drought Severity Index (PDSI) reconstructions (Cook et al., 2015) for the three European
regions, as defined by IPCC Sixth Assessment Report (AR6) (IPCC, 2021a; Iturbide et al., 2020): Northern Europe, Central
275 Europe, and the Mediterranean region. Furthermore, we show maps of the European summer VPD for the most extreme
positive years (1868, 1707, 1835) and most extreme negative years (1785, 1742, 1747) to investigate the spatial variability in
concordance with past historical data (Brázdil et al., 2013; Brooks and Glasspoole, 1922; Cook et al., 2015; Glaser, 2008;
Ionita et al., 2021; Marusek, 2010; Pauling et al., 2006; Trigo et al., 2009). Prior to this mapping, all VPD grid cells are centered
and standardized (z-transformation) to present z-anomalies for each grid cell.

280

3. Results and discussion

3.1 Vapor pressure deficit – $\delta^{18}\text{O}$ relationship

The network of $\delta^{18}\text{O}$ time series is significantly correlated with the European Summer VPD over the observational
period (i.e., 1900 – 1994). In Figure 3, we show the correlations of the individual $\delta^{18}\text{O}$ time series with the respective time
285 series of the grid cell from the calculated VPD of 20CRV3 (Slivinski et al., 2019). High values of significant correlations are
reached between the local summer VPD and the $\delta^{18}\text{O}$ time series (Figure 3). We found that 23 of the 26 sites show significant
correlations with local summer VPD (i.e., from the closest grid point) at the 95% confidence level, with most of these sites
being located in France, Spain, Germany, Scandinavia, and Great Britain. One time series from Turkey, one from Finland, and
one from Bulgaria do not have a significant correlation with local summer VPD (Figure 3). We note, however, that tree rings
290 from south-eastern Europe (e.g., Turkey, Bulgaria) may be more sensitive to spring VPD rather than summer VPD as
demonstrated by a former study (Heinrich et al., 2013). In addition, we notice that there is no influence of the tree species
used and no influence of the altitude of sampled trees on the correlations found (Figure 3, Table 1 (Balting et al., 2021)). Based

on these results and the relationship between $\delta^{18}\text{O}$ and VPD variability depicted above, we can argue that $\delta^{18}\text{O}$ in tree-ring cellulose can be used as a reliable proxy to perform the reconstruction of VPD for the summer months (JJA).

295

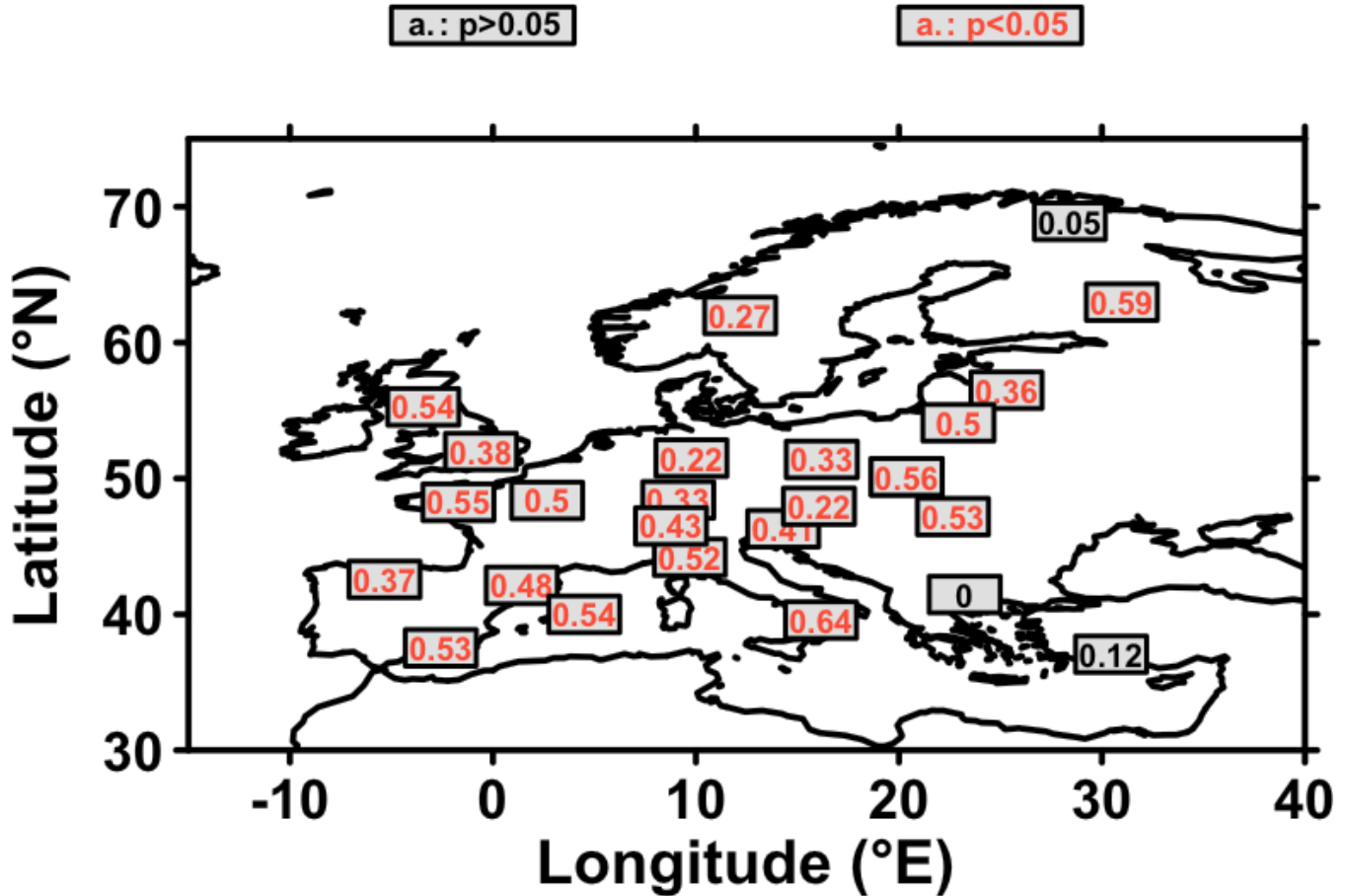
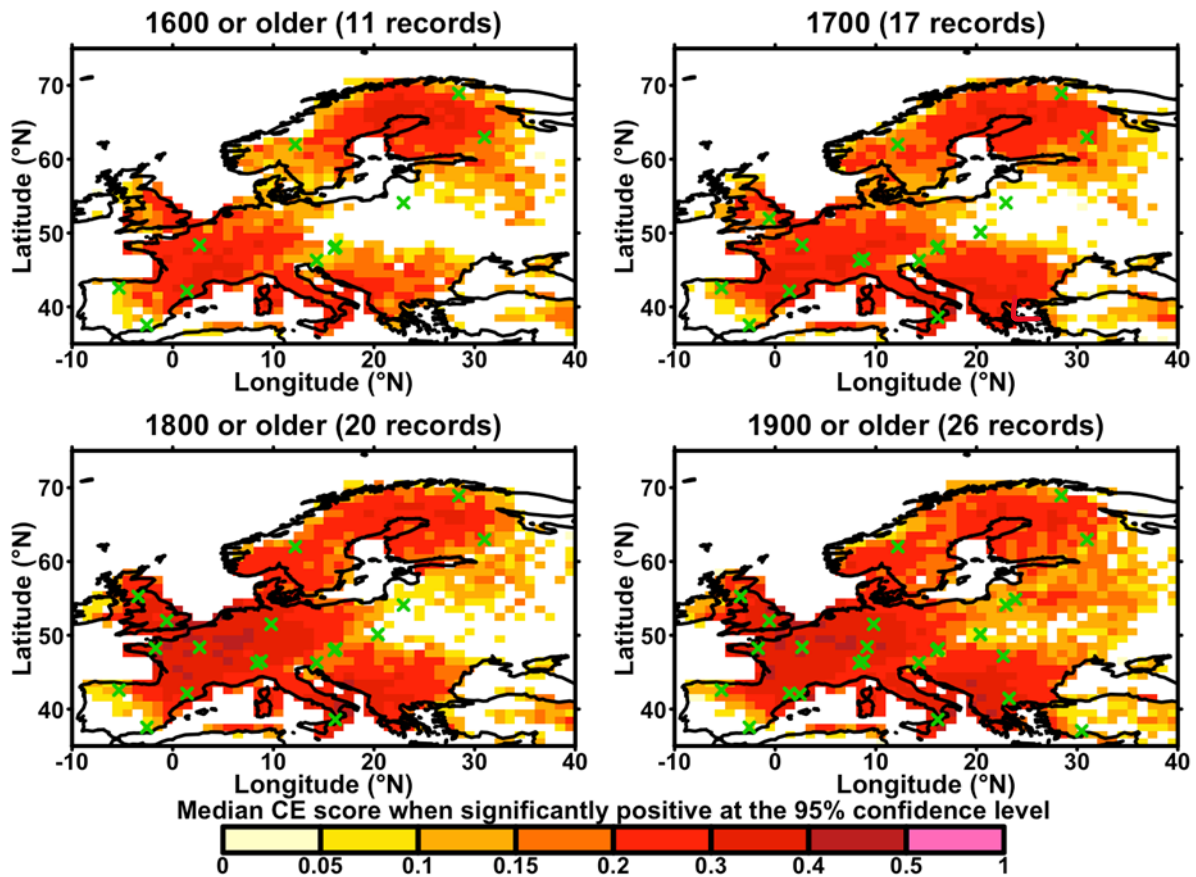


Figure 3: Correlation of the $\delta^{18}\text{O}$ time series with local summer VPD for the period 1900 to 1994. For each tree ring data, the correlation is computed with the time series from the closest grid point. The significance of correlations is calculated using a Student t-test for correlation with corrected degrees of freedom from time series as in McCarthy et al., (2015) and Michel et al., (2020). Significant correlations at the 95% confidence level are highlighted in red (p<0.05).
300

3.2 Validation statistics

Since we used a nesting approach in our study (section 2.5), we made 13 successions of RF models over space in total (section 2.5), each starting from time steps where at least one time series from the tree-ring network becomes available (see section 2.5). The S_{CE} scores (see section 2.5) are shown in Figure 4 for four selected time steps (1600 – 1699, 1700 – 1799, 1800 – 1899, and 1900 – 1999).
305



310 **Figure 4: The median Nash–Sutcliffe S_{CE} for four different time slices.** The colored areas show the regions where the model set up has a suitable quality, which was tested with a one-sided Student's t-test for the average of 30 S_{CE} scores obtained for testing samples ($p < 0.05$, section 2.5). For the sake of graphical representation for each time slice plotted here, median S_{CE} scores were averaged over the corresponding nested time frames, when significant for all. Locations of available records for each time slice are given by green crosses (see Table 1).

315 For the first time step 1600 and older, S_{CE} scores indicate a satisfactory quality (section 2.5) for the reconstruction of VPD for Northeast Spain, Italy, Greece, France, Germany, and large parts of Scandinavia (Figure 4a). These regions coincide with the locations of the eleven available time series for this time frame. For 1700 or older, when our $\delta^{18}O$ network has increased to 16 time series, the validation scores became higher and the spatial coverage of grid points with a significantly robust reconstruction at the 95% confidence level now expands to some parts of Eastern Europe and the whole Scandinavian region (Figure 4b). A further improvement of the S_{CE} values can be observed for the time span until 1800 (Figure 4c), whereby the most noticeable feature is that Great Britain is now largely covered by grid points with a significantly robust reconstruction at the 95% confidence level. This improvement is due to the fact that another time series from Scotland has

been included in the analysis, for this time slice. Finally, for the last time step (i.e., 1900 – 1994), for which all 26 $\delta^{18}\text{O}$ time series are now available, an improvement in the spatial coverage of the reconstruction is found, in particular, a large gap in Eastern Europe is now robustly covered by our reconstruction, due to an additional time series from Romania, which became available from 1900 onwards (Figure 4d). It can also be noted that adjacent regions of Europe, such as parts of Turkey also have a suitable quality for reconstructing past VPD variability changes since a tree-ring series is available in this region. The overall spatial strength of the network is in Southern, Western, and Northern Europe, whereas Eastern Europe can only be partially covered. Therefore, only those grid cells with a satisfactory reconstruction performance (where the mean $S_{\{CE\}}$ scores are significantly positive at the 95% confidence level) will be included in the following analyses. In addition to the validation scores, we also computed and provided statistical uncertainties (Figure 5) in order to compute error bar estimates of the reconstruction (see section 2.3). Overall, the validation statistics passed the conventional verification tests, and the obtained statistical test results indicate that the reconstruction model was statistically sound and can be used for the reconstruction of summer VPD values at the European scale.

335

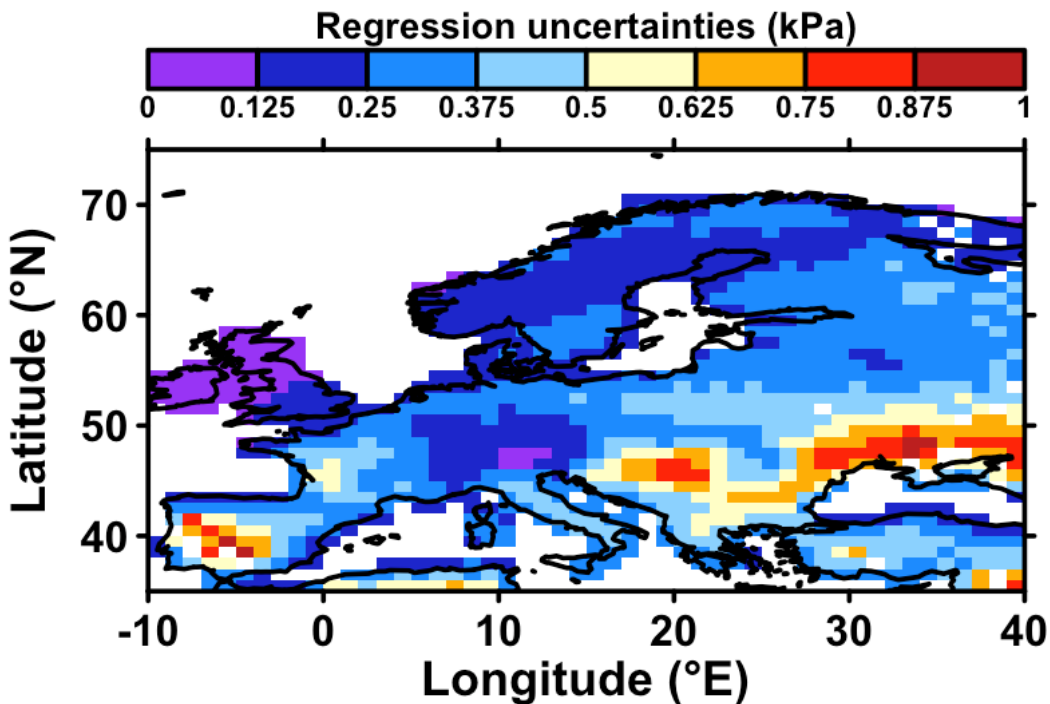


Figure 5: Regression uncertainties for each grid cell. Uncertainties are calculated as the time-averaged 10%-90% range of individual reconstructions from each grid point (for the longest period with reconstruction skills, see Figure 4).

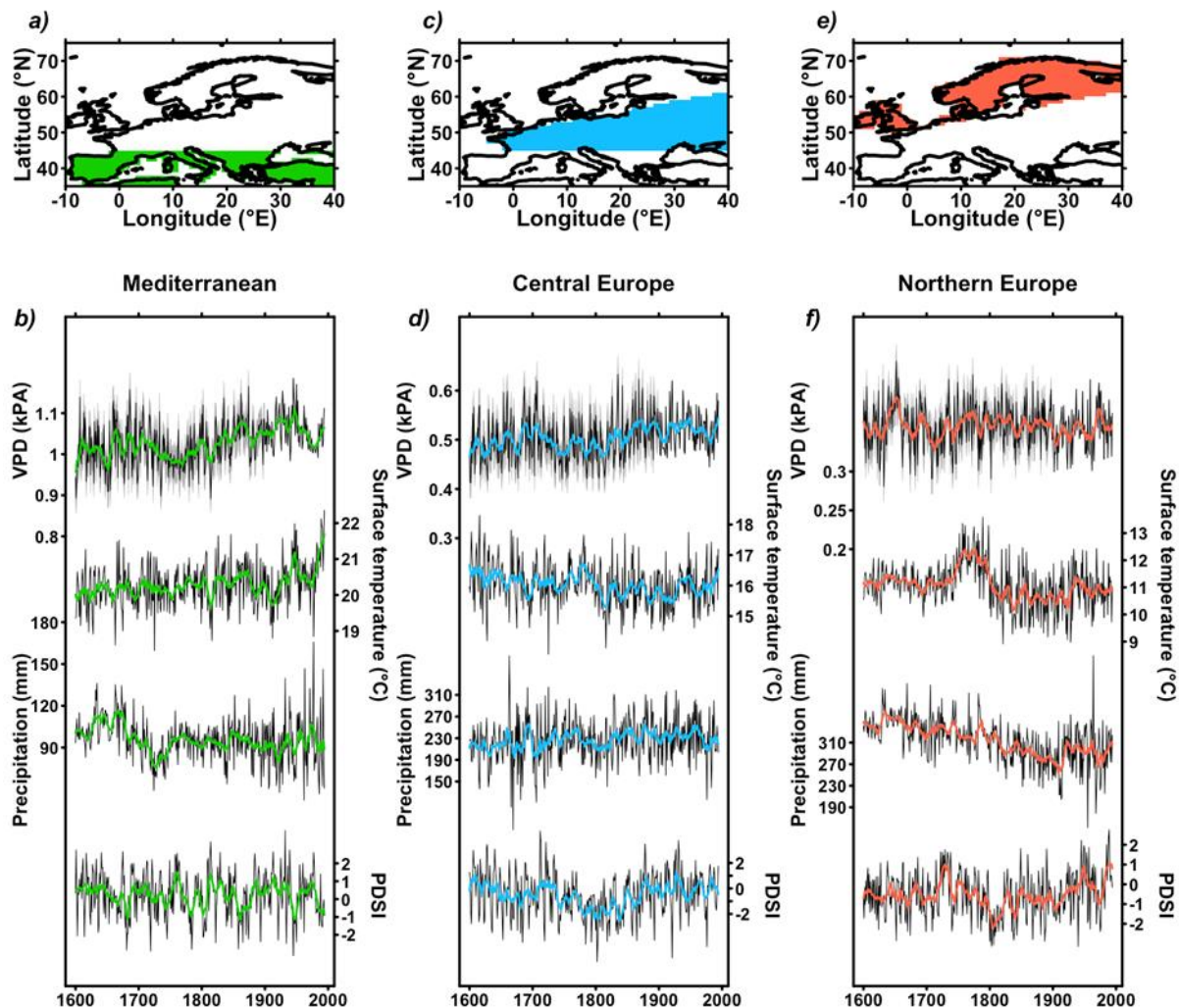
340

3.3 Temporal variability of the European summer VPD reconstruction

The VPD reconstruction for the Mediterranean region shows the largest VPD values and higher variability compared to the other two regions (Figure 6a, Figure 6b). It is noticeable that at the beginning of the reconstruction period (1610-1650), the VPD values decrease ($m = -0.0017 \text{ kPa}\cdot\text{year}^{-1}$; $0.05 < p\text{-value} < 0.01$, where m is the linear regression slope), which is followed by a VPD increase leading to an almost constant VPD level until ~ 1715 . After which, the VPD decreased steadily until 1761, where it remained at a similar level until 1773. This is followed by a short increase until ~ 1790 , after which VPD decreases again. The minimum of VPD value is also reached during this period (VPD=0.96 kPa for the year 1814). Around 1830, the VPD values start to increase again ($m = 0.0003 \text{ kPa}\cdot\text{year}^{-1}$; $0.05 < p\text{-value} < 0.01$). Furthermore, the reconstructed VPD time series shows similar variations as for Central Europe, but most pronounced in the last 150 years. Low periods of variability are shown for example between the end of the 19th century and the beginning of the 20th century as well as for the 1960s and 70s. In total, the three years with the lowest VPD z-anomalies in this region are 1735, 1814, and 1876 whereas the years with the highest VPD are 1682, 1686, and 1945.

The reconstructed VPD for Central Europe (Figure 6c, Figure 6d) shows that VPD increases from 1600 up to ~ 1700 ($m = 0.0007 \text{ kPa}\cdot\text{year}^{-1}$; $p\text{-value} < 0.01$). The maximum of the 30-year moving time series is reached in 1697 (VPD = 0.6398 kPa $> 2.4 \times \sigma$, where σ is the standard deviation of the time series). This increase is followed by a downward trend of VPD in Central Europe which ends in 1743, ($m = -0.0014 \text{ kPa}\cdot\text{year}^{-1}$; $0.01 < p\text{-value} < 0.05$), when the minimum VPD value was recorded. The period 1740 to 1760 is characterized by very low VPD values and the lowest 30-year rolling VPD. From this time on, the rolling average VPD is characterized by a rising trend ($m = 0.0002 \text{ kPa}\cdot\text{year}^{-1}$; $p\text{-value} < 0.01$), but low values are reached between 1790 and 1830. Furthermore, the VPD reconstruction is characterized by a significant 60 to 80 years variability, where the lowest values are reached during the periods 1890 to 1920 and 1960 to 1980 (Supplement Figure S3). In total, the three years with the lowest VPD in this region are 1814, 1838, and 1980 whereas the years with the highest VPD are 1687, 1707, and 1835.

The average VPD reconstruction for Northern Europe (Figure 6e, f) shows significant differences in variability as well as in the long-term mean. Northern Europe shows the lowest VPD of all three regions, which is due to the comparably low temperatures and high humidity in this area. The increase of VPD between 1620 and 1660 is significant ($m = 0.0017 \text{ kPa}\cdot\text{year}^{-1}$; $p\text{-value} < 0.01$), with the highest VPD value of the 400 years being reached in 1652 (VPD= 0.4619 kPa $> 2.7 \times \sigma$). However, we note that increase during 1675 – 1695 is not as long-lasting as the former increase from 1620 to 1660. The VPD values start to decrease again from the year 1700. The subsequent drop lasts until the 1720 to 1730 period, after which the time series shows further low-frequency variability and an upward tendency in the 30-year rolling average that lasts until the end of the 20th century ($m = 0.00002 \text{ kPa}\cdot\text{year}^{-1}$; $p\text{-value} < 0.01$). The three years with the lowest VPD in this region are 1632, 1674, and 1802 whereas the years with the highest VPD are 1652, 1959, and 1973.

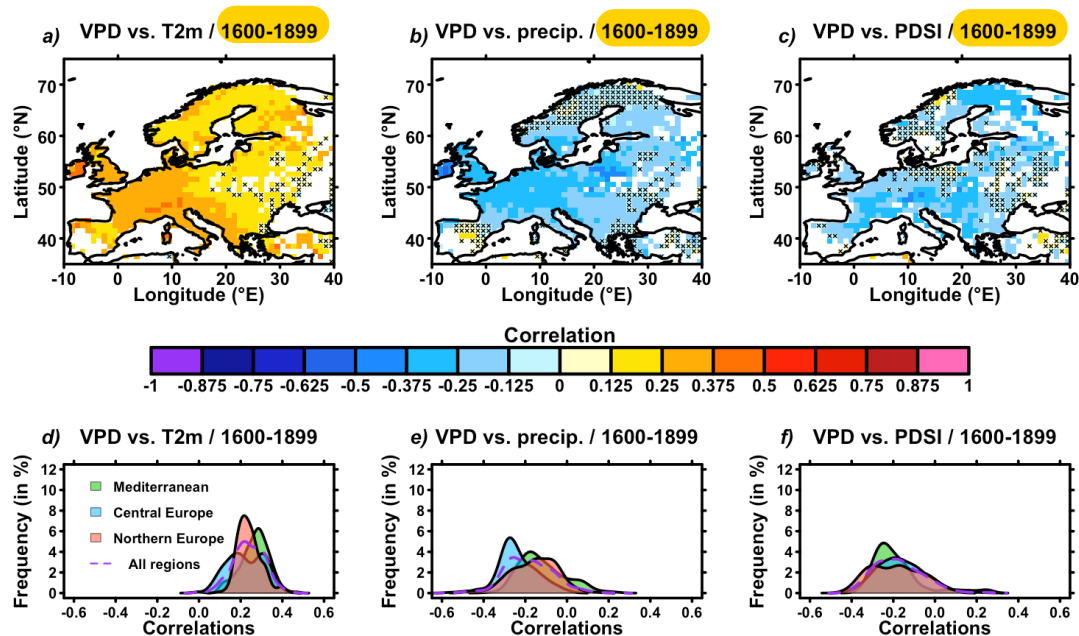


375 **Figure 6: Temporal variability of the VPD reconstruction.** Maps (a, c, e) give the location of regions investigated: Mediterranean (a, green), Central Europe (c, blue), and Northern Europe (f, red), following the IPCC AR6 definition (Iturbide et al., 2020). Area-averaged reconstructed time series (b, d, f) for (top to bottom): VPD (this study), surface temperature (Luterbacher et al., 2004), precipitation (Pauling et al., 2006), and PDSI (Cook et al., 2015) for the period 1600-1994, for the same three regions. For VPD timeseries in b, d, f, grey-shaded areas give the range of spatially averaged VPD uncertainties
380 from Figure 5 at the annual timescale, where values are spatio-temporally filtered based on reconstruction skills (Figure 4).

3.4 Validation of the VPD reconstruction by comparison with other datasets

In order to test the feasibility of our VPD reconstruction, in the following two sub-sections we compare the spatio-temporal variability of our VPD reconstruction with other datasets available for the same time span. Time series from Figure

385 6b, d, f show some interesting similarities between our summer VPD reconstruction and former ones based on different climatic variables (e.g., precipitation, temperature, drought indicators) (Cook et al., 2015; Luterbacher et al., 2004; Pauling et al., 2006). For the overlap period of these reconstructions (1600-1994), we find consistent positive correlations with area-averaged reconstructed summer temperatures at 2 meters (T2m, (Luterbacher et al., 2004)). The obtained correlations vary between $r=0.36$ ($p<0.01$) for the Mediterranean region, $r=0.31$ ($p<0.01$) for central Europe, and $r=0.38$ ($p<0.01$) for northern Europe 390 (Figure 7). When averaged over the same three regions, an opposite (negative) relationship is found between our VPD reconstruction and a summer precipitation reconstruction (Pauling et al., 2006), where correlations for spatially averaged time series are: $r=-0.26$ ($p<0.01$) for the Mediterranean regions, $r=-0.35$ ($p<0.01$) for central Europe, and $r=-0.39$ ($p<0.01$) for northern Europe (Figure 7). The same results are found when we use a drought indicator, namely the Palmer Drought Severity Index (PDSI). In the case of PDSI, we find significant negative correlations for the three analysed regions, namely: $r=-0.39$ 395 ($p<0.01$) for the Mediterranean regions, $r=-0.24$ ($p<0.01$) for central Europe, and $r=-0.34$ ($p<0.01$) for northern Europe (Figure 7). Interestingly, the Mediterranean region has highest correlations on average for T2m whereas it has the lowest correlations for precipitation and PDSI.



400 **Figure 7: Comparison with former climate field reconstructions.** (a-c) Correlations between the VPD reconstruction from this study and other climate reconstructions: a) temperature at two meters (T2m) (Luterbacher et al., 2004); b) precipitation (precip) (Pauling et al., 2006); and c) Palmer Drought Severity Index (PDSI) (Cook et al., 2015); for the period 1600-1994. Black crosses indicate no significance at the 95% confidence level. (d-f) Distribution of correlations from a-c for

the same three variables, respectively, for the three regions investigated: Mediterranean (green), Central Europe (blue),
405 Northern Europe (red), and all regions (purple dashed line), following IPCC AR6 (Iturbide et al., 2020), Figure 5).

The spatial correlations with other (paleo)climate reconstructions (the temperature at 2 meters, T2m (Luterbacher et al.,
2004); precipitation (Pauling et al., 2006); and PDSI (Cook et al., 2015)) are given in Figure 7a-c. It appears that for all three
variables, significant correlations are found, with a focus on western and central Europe, which are the areas with the highest
410 tree-ring data coverage (Figure 1, Table 1) and show the highest S_{CE} validation scores (Figure 4). Taking into account the
size of the spatial extension (the whole of Europe) and the time span (400 years) of the correlated data sets, the modest
(lower/higher than +/- 0.2), but significant correlation coefficients represent a satisfactory result. Therefore, the significant
correlations found for most regions highlight the important accordance and consistency between the summer VPD
reconstruction and former summer climate reconstructions (Cook et al., 2015; Luterbacher et al., 2004; Pauling et al., 2006).

415

3.5 Comparison of the temporal variability with other reconstructions

In this section, we compare the temporal variability of VPD with existing reconstructions of summer temperature
(Luterbacher et al., 2004), precipitation (Pauling et al., 2006), and drought (PDSI) reconstruction (Cook et al., 2015) in Figure
6, 7, and 8.

420 For Northern Europe, the characteristics of VPD until 1700 show little resemblance with the reconstructions of
precipitation and temperature (Figure 6 e, f). However, the PDSI indicates dry conditions for the time of the maximum VPD
in 1652 (Figure 6d). Furthermore, the decrease of VPD between 1700 and 1730 is shown as a wet period in the drought
reconstruction, which could be a possible explanation for these low values. From 1730 to 1800, the observed strong temperature
increase is visible in VPD only partly. A possible reason for this could be the concurrent increase in summer precipitation.
425 Since the temperature and precipitation changes in this region have similar trends, it is difficult to detect the characteristics of
the two variables in the VPD time series.

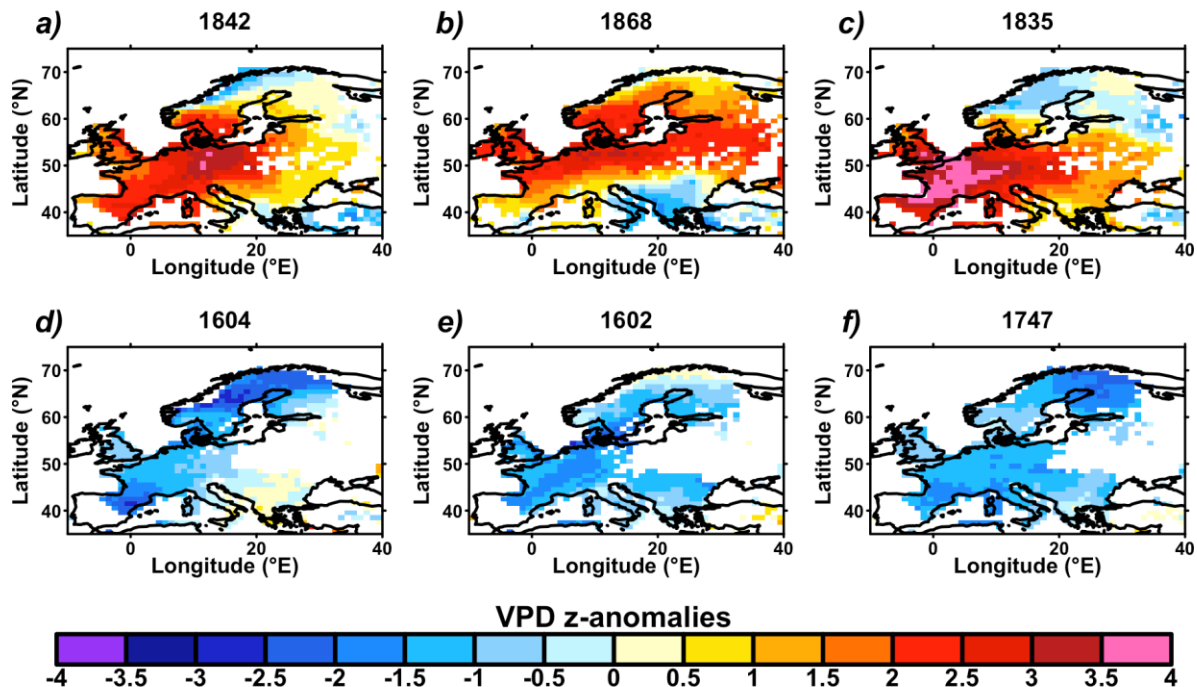
For Central Europe, the increase of the VPD until 1700 cannot be explained by the temperature or precipitation
reconstruction (Figure 6d). The 30-year running means of both time series show diverging trends. Nevertheless, the
reconstruction of the PDSI also shows a trend towards drier conditions from 1670 to 1690 (Figure 6d). However, before the
430 end of the 17th century, the data indicates a wetting trend. Afterwards, the periods of high and low temperature and precipitation
match well with the corresponding periods of high and low VPD. For example, a simultaneous drop in temperature and
precipitation between 1730 and 1745 is also present in the VPD time series. From 1800 onward, the VPD follows closely the
pattern of temperature (Supplement Figure S3). However, the variability of the VPD time series is also influenced by the
precipitation variability. The precipitation shows strong interannual variability from the second half of the 19th century, but the
435 magnitude is weaker than in the VPD or the temperature time series. The temperature, precipitation, and VPD reconstructions
show similar patterns, it gets warmer, there is less precipitation, and the VPD increases in summer. The PDSI, on the other
hand, shows a wetting trend from 1800 onwards. We suggest that this could be based on the accumulation processes of

precipitation in the preceding months which is represented by the PDSI (Alley, 1984). This could compensate for the increasing temperature and the decreasing precipitation in summer.

440 For the Mediterranean area, the summer of 1884 is an extreme event in the temperature time series, as it shows the second coldest temperatures for this region in the last 400 years (Figure 6b). The variability of periods with high and low temperatures are almost identical to the corresponding periods of the VPD time series. During the period 1600 – 1730, the summer VPD reconstruction present a high variability, similar variability being observed and for the precipitation reconstruction. After which, the summer VPD reconstruction present a slow decreasing trend, similar to the temperature
445 reconstruction. Since the decrease in precipitation is almost linear in the 30-year mean from 1850, we suggest that, comparatively, the variability of temperatures can be clearly observed in the VPD time series. A similar situation is also described by the drought reconstruction for the Mediterranean area (Figure 6b). Thus, the reconstructed PDSI of Cook et al. 2015 shows wetter conditions towards the middle of the 18th century, which is complemented by the low VPD values for this
450 the onset around 1790. Furthermore, the year 1814 is also the year with the wettest conditions in the PDSI time series. After ~1850, the anti-correlation between temperature/VPD and the PDSI is again evident, so that variability is also visible.

3.6 Extreme years in the VPD reconstruction and comparison of past/historical data

To illustrate the spatial variability of our VPD reconstruction we selected three of the driest summers (1842, 1868, and
455 1835) and three of the wettest summers (1604, 1602, and 1747), when considering time frames with significantly positive $S_{\{CE\}}$ scores at the 95% confidence level for each grid point (Figure 4). We compared their spatial variability (Figure 8) with respect to other available reconstructions or documentary pieces of evidence, at the European level, to validate once again the occurrence of the extreme events in our reconstruction. Since VPD variability and mean state differ strongly for different latitudes, these six extreme years were selected using spatially-averaged normalized VPD values (i.e., z-anomalies). Year 1747
460 is part of a relatively wet period which correspond to strongly decreasing PDSI (Cook et al., 2015; Ionita et al., 2021) for Europe on average, notably for northernmost regions (Figure 6f) as also suggested by Figures 8f. Contrarily, the summer of 1835 is characterized by positive anomalies over south, western, and central Europe, with the highest VPD anomalies over France, which is in concordance with the extremely hot summer condition in France during that summer (Marusek, 2010). During the summer of 1835, in Paris, France was recorded 41 hot days and 11 very hot days (Marusek, 2010). Heat and dryness
465 conditions were also registered in Belgium, England, and Switzerland in 1835 (Marusek, 2010), which is in concordance with our results (Figure 8c). Summer 1868 is characterized by positive anomalies over the western, central-eastern, and northern parts of Europe (Figure 6a). Documentary data indicate a hot and dry summer in England (e.g. on 21 July 1835 in London was recorded a temperature of 34.1°C) (Marusek, 2010).



470 **Figure 8: Spatial pattern of VPD anomalies for selected years.** Values of each grid cell are VPD z-anomalies (standardized
 and centered), with respect to the whole period of study (1600-1994). Years were selected as the three with the highest VPD
 z-anomalies (a-c, a is the highest) and the three with lowest VPD z-anomalies (d-f, d is the lowest) for preindustrial data (1600-
 1899). Time series only include years where $S_{\{CE\}}$ scores are significantly positive at the 95% confidence level (see Figure
 4).

475

Interestingly, none of the three cases with high VPD anomalies (Figure 8a-c) has overall spatially consistent positive
 values over the continent compared to low VPD cases (Figure 8d-f). Strong positive anomalies appeared over the western and
 northern parts of Europe in 1868 (Figure 8a), and western to central Europe in 1707 and 1835 (Figures 8b and 8c). In all three
 cases, these large positive anomalies are accompanied by negative anomalies in other regions (in general Northeast and
 480 Southeast Europe, Figure 8) and form a significant contrast over the continent. Oppositely, the three wettest years happened
 mainly as a large and spatially consistent set of negative VPD z-anomalies, where only scattered positive values occurred in a
 few regions (Figure 8d-f).

4. Limitations of the reconstruction

485

The $\delta^{18}O$ network used in our study (Table 1, Figure 1) is characterized by specific limitations that inevitably influence
 the quality of the reconstruction presented here. It is likely that the reconstruction may provide some level of sample sites over-
 representation in Central and Western Europe compared to the ones from Southeast, East, and Northern Europe as shown in

Figure 1. These spatial distribution characteristics of sites can also be seen in the validation statistics, where the regions with a good sample density show higher validation scores (Section 3.2). Therefore, further time series from uncovered regions may help in improving the quality and the spatial extent of our reconstruction. Besides the $\delta^{18}\text{O}$ climate signal, the observational/reanalysis data of VPD is given by the ensemble mean of 20CRV3 (Slivinski et al., 2019) for the period 1900 to 1994. Even though the quality and quantity of instrumental data available during this period are comparatively good, the ensemble mean can only represent the variability and diversity of the reanalysis with 80 ensemble members to a limited extent.

In our study, the reconstruction is based on the application of the RF algorithm calibrated and evaluated over the period 1900 to 1994. The model is therefore trained to represent exactly this period. Thus, when this model is applied to the previous years, we assume stationarity between the VPD variability and the proxy records, as is generally the case for climate reconstructions (Cook et al., 2015). Since the climate system is not stationary, the assumption of stationarity must be included as a potential source of error. However, the RF approach can represent non-linearities which is not possible with the classical approaches, for example, Principal Component Regression (Cook et al., 2015). Therefore, we compared our reconstruction with other available observational, historical, and proxy based reconstructed data in order to assess errors.

Finally, even if the nested reconstruction approach is used by default for reconstructions (Cook et al., 2007; Freund et al., 2019; Luterbacher et al., 2004; Pauling et al., 2006) to cover the longest possible time range, it is important to check the quality of the model for the respective time range. Therefore, we recommend considering the validation scores for the considered time periods which are also uploaded in the repository.

505

5. Conclusion & Outlook

Here, we present the first gridded reconstruction of the European summer VPD over the past 400 years, a dataset which was produced to cover a large knowledge gap about past European VPD variability. The validation statistics performed to obtain our summer VPD reconstruction, passed all of the conventional verification tests (e.g., Nash–Sutcliffe model efficiency coefficient (S_{CE})), and the obtained statistical test results indicate that the reconstruction model was statistically robust. Thus, we can present, the first reconstructions over 400 years of the summer VPD, at the European level. Our spatial reconstruction of summer VPD conditions over Europe, based on tree-ring $\delta^{18}\text{O}$ records provides evidence of historical changes and a unique long-term context for recent trends and variability of the summer VPD. Moreover, our reconstruction helps to analysed the spatio-temporal variability of summer VPD in a long-term context emphasizing the local and regional impacts of the current climate change.

The obtained results indicate that the past variability of VPD is different for the three regions we investigated, namely: Northern Europe, Central Europe, and the Mediterranean. Over the Mediterranean region were recoded much higher summer VPD values compared with to the other two regions, for the analysed period. The lowest summer VPD values were found for Northern Europe, which can be explained by lower temperatures and higher humidity in this area. Similar results were found and for the variability of the summer VPD.

520

The comparison of our summer VPD reconstruction with other climate datasets reveal consistent positive correlations with summer temperatures but negative correlations with summer precipitation and a drought indicator in different European regions, demonstrating agreement with previous climate reconstructions, especially in western and central Europe over a 400-year period.

525 Our summer VPD reconstruction is also validated by examining the occurrence of the extreme years, the extremely hot and dry summers coincide with high VPD anomalies, while the extremely wet summers coincide with low VPD anomalies. Interestingly, the high VPD anomaly years show spatial variability with large positive anomalies in specific regions, while the wettest years display consistent negative VPD anomalies over the continent.

530 Furthermore, the interdisciplinary use of the data should be emphasized, as VPD is a crucial parameter for many climatological processes. As a logical next step, the regional and temporal boundaries of the reconstruction can be extended by using more and longer $\delta^{18}\text{O}$ time series from tree-ring cellulose. It is also possible to disentangle the influence of solar events on the VPD on the local, regional, and continental scales.

535

540

545

550

555 **Contributions**

D.F.B conceived the ideas and designed the methodology together with S.L.L.M. and V.N. D.F.B analyzed the data, drafted and led the writing of the manuscript with significant inputs from S.L.L.M, M.I., V.N., G.H., M.F., G.H.S., D.N.S., and G.L. All authors contributed critically to the drafts and gave final approval for publication.

560 **Data and Code availability**

The gridded reconstructed summer VPD over the last 400 years, at the European level, is available here: <https://doi.org/10.5281/zenodo.5958836> (Balting, D. F. et al., 2022). The ISONET oxygen isotope data can be accessed at GFZ Data Services: <https://doi.org/10.5880/GFZ.4.3.2023.001>. The time series of the individual sample sites can be request by the corresponding authors of the mentioned studies in the proxy network Section. The climate data from 20CRv3 is freely available. The postprocessing of the model and reanalysis output data has been done with the Climate Data Operators (Schulzweida, 2019) and the corresponding Python binding. Furthermore, the reconstruction of the VPD have been done with a modified version of the ClimIndRec version 1.0 scripts (<https://zenodo.org/record/5716236#.YZkyyi2ZOL8>) in R (version 4.0.2). The required R packages (glmnet, pls, randomForest, ncd4 and dependencies) are freely available.

570 **Competing interests**

The authors declare that there is no conflict of interest.

Acknowledgment

Funding by the PalEX Project (AWI Strategy Fund) is greatly acknowledged. GL and MI are supported by Helmholtz funding through the joint program "Changing Earth - Sustaining our Future" (PoF IV) program of the AWI. Funding by the Helmholtz Climate Initiative - REKLIM is gratefully acknowledged. VN was partially supported by a grant of the Ministry of Research, Innovation and Digitization, CNCS/CCCDI – UEFISCDI, project number PN-III-P1-1.1-PD-2019-0469, within PNCDI III. All but four tree-ring stable isotope chronologies were established within the project ISONET supported by the European Union (EVK2-CT-2002-00147 ‘ISONET’). We want to thank all participants of the ISONET project (L. Andreu, Z. Bednarz, F. Berninger, T. Boettger, C. M. D’Alessandro, J. Esper, N. Etien, M. Filot, D. Frank, M. Grabner, M. T. Guillemin, E. Gutierrez, M. Haupt, E. Hilarvuori, H. Jungner, M. Kalela-Brundin, M. Krapiec, M. Leuenberger, H.H. Leuschner, N. J. Loader, V. Masson-Delmotte, A. Pazdur, S. Pawelczyk, M. Pierre, O. Planells, R. Pukiene, C. E. Reynolds-Henne, K. T. Rinne, Saracino, M. Saurer, E. Sonninen, M. Stievenard, V. R. Switsur, M. Szczepanek, E. Szychowska-Krapiec, L. Todaro, K. Treydte, J. S. Waterhouse, and M. Weigl). The data from Turkey, Slovenia and Southwest Germany were produced with the EU-funded project MILLENNIUM (GOCE 017008-2‘MILLENNIUM’), special thanks to T. Levanic and R. Touchan. The tree-ring stable isotope chronologies from Bulgaria were established with support of the German Research Foundation DFG (HE3089-1, GR 1432/11-1) and in cooperation with the administration of Pirin National Park, Bulgaria. Furthermore, we want to thank Paul Gierz and Christian Stepanek for technical support.

- Alley, W. M.: The Palmer Drought Severity Index: Limitations and Assumptions, *J. Clim.*, 23, 1100–1109 [online] Available from: <http://journal.um-surabaya.ac.id/index.php/JKM/article/view/2203>, 1984.
- Andreu-Hayles, L., Ummenhofer, C. C., Barriendos, M., Schleser, G. H., Helle, G., Leuenberger, M., Gutiérrez, E. and Cook, E. R.: 400 Years of summer hydroclimate from stable isotopes in Iberian trees, *Clim. Dyn.*, 49(1–2), 143–161, doi:10.1007/s00382-016-3332-z, 2017.
- Bair, E. H., Calfa, A. A., Rittger, K. and Dozier, J.: Using machine learning for real-time estimates of snow water equivalent in the watersheds of Afghanistan, *Cryosphere*, 12(5), doi:10.5194/tc-12-1579-2018, 2018.
- Balting, D. F., Ionita, M., Wegmann, M., Helle, G., Schleser, G. H., Rimbu, N., Freund, M. B., Heinrich, I., Caldarescu, D. and Lohmann, G.: Large-scale climate signals of a European oxygen isotope network from tree rings, *Clim. Past*, 17(3), doi:10.5194/cp-17-1005-2021, 2021.
- Barbour, M. M.: Stable oxygen isotope composition of plant tissue: A review, *Funct. Plant Biol.*, 34(2), doi:10.1071/FP06228, 2007.
- Barbour, M. M., Roden, J. S., Farquhar, G. D. and Ehleringer, J. R.: Expressing leaf water and cellulose oxygen isotope ratios as enrichment above source water reveals evidence of a Péclet effect, *Oecologia*, 138(3), doi:10.1007/s00442-003-1449-3, 2004.
- Barkhordarian, A., Saatchi, S. S., Behrangi, A., Loikith, P. C. and Mechoso, C. R.: A Recent Systematic Increase in Vapor Pressure Deficit over Tropical South America, *Sci. Rep.*, 9(1), doi:10.1038/s41598-019-51857-8, 2019.
- Behrangi, A., Fetzer, E. J. and Granger, S. L.: Early detection of drought onset using near surface temperature and humidity observed from space, *Int. J. Remote Sens.*, 37(16), doi:10.1080/01431161.2016.1204478, 2016.
- Belgiu, M. and Drăgu, L.: Random forest in remote sensing: A review of applications and future directions, *ISPRS J. Photogramm. Remote Sens.*, 114, doi:10.1016/j.isprsjprs.2016.01.011, 2016.
- Boettger, T., Haupt, M., Konller, K., Weise, S. M., Waterhouse, J. S., Rinne, T., Loader, N. J., Sonninen, E., Jungner, H., Masson-Delmotte, V., Stievenard, M., Guillemin, M.-T., Pierre, M., Pazdur, A., Leuenberger, M., Filot, M., Saurer, M., Reynolds, C. E., Helle, G. and Schleser, G. H.: Wood Cellulose Preparation Methods and Mass Spectrometric Analyses of $\delta^{13}\text{C}$, $\delta^{18}\text{O}$, and Nonexchangeable $\delta^2\text{H}$ Values in Cellulose, Sugar, and Starch: An Interlaboratory Comparison, *Anal. Chem.*, 79(12), 4603–4612, doi:10.1021/ac0700023, 2007.
- Brázdil, R., Dobrovolný, P., Trnka, M., Kotyza, O., Řezníčková, L., Valášek, H., Zahradníček, P. and Štěpánek, P.: Droughts in the Czech Lands, 1090–2012 AD, *Clim. Past*, 9(4), doi:10.5194/cp-9-1985-2013, 2013.
- Breiman, L.: Random Forests, *Mach. Learn.*, 45, 5–32, doi:10.1109/ICCECE51280.2021.9342376, 2001.
- Brooks, C. E. P. and Glasspoole, J.: The drought of 1921 in the British Isles, *Mon. Weather Rev.*, 50(2), 93–93, doi:10.1175/1520-0493(1922)50<93a:tdoitb>2.0.co;2, 1922.
- Buckley, T. N.: How do stomata respond to water status?, *New Phytol.*, 224(1), doi:10.1111/nph.15899, 2019.

- Churakova Sidorova, O. V., Corona, C., Fonti, M. V., Guillet, S., Saurer, M., Siegwolf, R. T. W., Stoffel, M. and Vaganov, E. A.: Recent atmospheric drying in Siberia is not unprecedented over the last 1,500 years, *Sci. Rep.*, 10(1), 625 doi:10.1038/s41598-020-71656-w, 2020.
- Cook, E. R., Seager, R., Cane, M. A. and Stahle, D. W.: North American drought: Reconstructions, causes, and consequences, *Earth Sci. Rev.*, 81(1), 93–134, doi:10.1016/j.earscirev.2006.12.002, 2007.
- Cook, E. R., Seager, R., Kushnir, Y., Briffa, K. R., Büntgen, U., Frank, D., Krusic, P. J., Tegel, W., van der Schrier, G., Andreu-Hayles, L., Baillie, M., Baittinger, C., Bleicher, N., Bonde, N., Brown, D., Carrer, M., Cooper, R., Čufar, K., 630 Dittmar, C., Esper, J., Griggs, C., Gunnarson, B., Günther, B., Gutierrez, E., Haneca, K., Helama, S., Herzig, F., Heussner, K.-U. U., Hofmann, J., Janda, P., Kontic, R., Köse, N., Kyncl, T., Levanič, T., Linderholm, H., Manning, S., Melvin, T. M., Miles, D., Neuwirth, B., Nicolussi, K., Nola, P., Panayotov, M., Popa, I., Rothe, A., Seftigen, K., Seim, A., Svarva, H., Svoboda, M., Thun, T., Timonen, M., Touchan, R., Trotsiuk, V., Trouet, V., Walder, F., Ważny, T., Wilson, R., Zang, C., Schrier, G. V. Der, Andreu-Hayles, L., Baillie, M., Baittinger, C., Bleicher, N., Bonde, N., Brown, 635 D., Carrer, M., Cooper, R., Eufar, K., Dittmar, C., Esper, J., Griggs, C., Gunnarson, B., Günther, B., Gutierrez, E., Haneca, K., Helama, S., Herzig, F., Heussner, K.-U. U., Hofmann, J., Janda, P., Kontic, R., Köse, N., Kyncl, T., Levaniè, T., Linderholm, H., Manning, S., Melvin, T. M., Miles, D., Neuwirth, B., Nicolussi, K., Nola, P., Panayotov, M., Popa, I., Rothe, A., Seftigen, K., Seim, A., Svarva, H., Svoboda, M., Thun, T., Timonen, M., et al.: Old World megadroughts and pluvials during the Common Era, *Sci. Adv.*, e1500561 6(10), 1–10, doi:10.1126/sciadv.1500561, 640 2015.
- Craig, H.: Isotopic standards for carbon and oxygen and correction factors for mass-spectrometric analysis of carbon dioxide, *Geochim. Cosmochim. Acta*, 12(1–2), doi:10.1016/0016-7037(57)90024-8, 1957.
- Dai, A.: Increasing drought under global warming in observations and models, *Nat. Clim. Chang.*, 3(1), 52–58, doi:10.1038/nclimate1633, 2013.
- 645 Davies, D. and Loader, N. J.: An evaluation of english oak earlywood vessel area as a climate proxy in the UK, *Dendrochronologia*, 64, doi:10.1016/j.dendro.2020.125777, 2020.
- Delcroix, T., Michel, S. L. L., Swingedouw, D., Malaizé, B., Daniau, A.-L., Abarca-del-Rio, R., Caley, T. and Sémah, A.-M.: Clarifying the role of ENSO on Easter Island precipitation changes: Potential environmental implications for the last millennium. XX, XX-XX (202X), *Paleoceanography and Paleoclimatology*, under revi, 2022.
- 650 Etien, N., Daux, V., Masson-Delmotte, V., Stievenard, M., Bernard, V., Durost, S., Guillemin, M. T., Mestre, O. and Pierre, M.: A bi-proxy reconstruction of Fontainebleau (France) growing season temperature from A.D. 1596 to 2000, *Clim. Past*, 4(2), doi:10.5194/cp-4-91-2008, 2008.
- Ferrio, J. P. and Voltas, J.: Carbon and oxygen isotope ratios in wood constituents of *Pinus halepensis* as indicators of precipitation, temperature and vapour pressure deficit, *Tellus, Ser. B Chem. Phys. Meteorol.*, 57(2), doi:10.1111/j.1600- 655 0889.2005.00137.x, 2005.
- Fletcher, A. L., Sinclair, T. R. and Allen, L. H.: Transpiration responses to vapor pressure deficit in well watered “slow-

- wilting” and commercial soybean, *Environ. Exp. Bot.*, 61(2), doi:10.1016/j.envexpbot.2007.05.004, 2007.
- 660 Freund, M. B., Henley, B. J., Karoly, D. J., McGregor, H. V., Abram, N. J. and Dommenges, D.: Higher frequency of Central Pacific El Niño events in recent decades relative to past centuries, *Nat. Geosci.*, 12(6), doi:10.1038/s41561-019-0353-3, 2019.
- Fritts, H. C.: *Tree Rings and Climate*, Academic Press, London., 1976.
- Gagen, M., Battipaglia, G., Daux, V., Duffy, J., Dorado-Liñán, I., Hayles, L. A., Martínez-Sancho, E., McCarroll, D., Shestakova, T. A. and Treydte, K.: Climate Signals in Stable Isotope Tree-Ring Records BT - Stable Isotopes in Tree Rings: Inferring Physiological, Climatic and Environmental Responses, in *Stable Isotopes in Tree Rings. Tree Physiology*, edited by R. T. W. Siegwolf, J. R. Brooks, J. Roden, and M. Saurer, pp. 537–579, Springer International Publishing, Cham., 2022.
- 665 Glaser, R.: *Klimageschichte Mitteleuropas: 1200 Jahre Wetter, Klima, Katastrophen*, Primus Verlag, Darmstadt., 2008.
- González-González, B. D., Vázquez-Ruiz, R. A. and García-González, I.: Effects of climate on earlywood vessel formation of *quercus robur* and *q. Pyrenaica* at a site in the northwestern iberian peninsula, *Can. J. For. Res.*, 45(6), doi:10.1139/cjfr-2014-0436, 2015.
- 670 Good, S. P., Noone, D. and Bowen, G.: Hydrologic connectivity constrains partitioning of global terrestrial water fluxes, *Science* (80-.), 349(6244), doi:10.1126/science.aaa5931, 2015.
- Grossiord, C., Buckley, T. N., Cernusak, L. A., Novick, K. A., Poulter, B., Siegwolf, R. T. W., Sperry, J. S. and McDowell, N. G.: Plant responses to rising vapor pressure deficit, *New Phytol.*, 226(6), doi:10.1111/nph.16485, 2020.
- 675 Hafner, P., McCarroll, D., Robertson, I., Loader, N. J., Gagen, M., Young, G. H. F., Bale, R. J., Sonninen, E. and Levanič, T.: A 520 year record of summer sunshine for the eastern European Alps based on stable carbon isotopes in larch tree rings, *Clim. Dyn.*, 43(3), 971–980, doi:10.1007/s00382-013-1864-z, 2014.
- Haupt, M., Weigl, M., Grabner, M. and Boettger, T.: A 400-year reconstruction of July relative air humidity for the Vienna region (eastern Austria) based on carbon and oxygen stable isotope ratios in tree-ring latewood cellulose of oaks (*Quercus petraea* Matt. Liebl.), *Clim. Change*, 105(1), 243–262, doi:10.1007/s10584-010-9862-1, 2011.
- 680 Heinrich, I., Touchan, R., Dorado Liñán, I., Vos, H. and Helle, G.: Winter-to-spring temperature dynamics in Turkey derived from tree rings since AD 1125, *Clim. Dyn.*, 41(7–8), doi:10.1007/s00382-013-1702-3, 2013.
- Helama, S., Läänelaid, A., Raisio, J., Mäkelä, H. M., Hilasvuori, E., Jungner, H. and Sonninen, E.: Oak decline analyzed using intraannual radial growth indices, $\delta^{13}\text{C}$ series and climate data from a rural hemiboreal landscape in southwesternmost Finland, *Environ. Monit. Assess.*, 186(8), doi:10.1007/s10661-014-3731-8, 2014.
- 685 Hersbach, H., Bell, B., Berrisford, P., Hirahara, S., Horányi, A., Muñoz-Sabater, J., Nicolas, J., Peubey, C., Radu, R., Schepers, D., Simmons, A., Soci, C., Abdalla, S., Abellan, X., Balsamo, G., Bechtold, P., Biavati, G., Bidlot, J., Bonavita, M., De Chiara, G., Dahlgren, P., Dee, D., Diamantakis, M., Dragani, R., Flemming, J., Forbes, R., Fuentes, M., Geer, A., Haimberger, L., Healy, S., Hogan, R. J., Hólm, E., Janisková, M., Keeley, S., Laloyaux, P., Lopez, P., Lupu, C., Radnoti, G., de Rosnay, P., Rozum, I., Vamborg, F., Villaume, S. and Thépaut, J.-N.: The ERA5 global reanalysis, *Q. J. R.*
- 690

Meteorol. Soc., 146(730), 1999–2049, doi:<https://doi.org/10.1002/qj.3803>, 2020.

Hilasvuori, E., Berninger, F., Sonninen, E., Tuomenvirta, H. and Jungner, H.: Stability of climate signal in carbon and oxygen isotope records and ring width from Scots pine (*Pinus sylvestris* L.) in Finland, *J. Quat. Sci.*, 24(5), doi:10.1002/jqs.1260, 2009.

695 Ionita, M., Dima, M., Nagavciuc, V., Scholz, P. and Lohmann, G.: Past megadroughts in central Europe were longer, more severe and less warm than modern droughts, *Commun. Earth Environ.*, 2(1), 61, doi:10.1038/s43247-021-00130-w, 2021.

IPCC: Climate Change 2021: The Physical Science Basis. Contribution of Working Group I to the Sixth Assessment Report of the Intergovernmental Panel on Climate Change, edited by V. Masson-Delmotte, P. Zhai, A. Pirani, S. L. Connors, C. Péan, S. Berger, N. Caud, Y. Chen, L. Goldfarb, M. I. Gomis, M. Huang, K. Leitzell, E. Lonnoy, J. B. R. Matthews, T. K. Maycock, T. Waterfield, O. Yelekçi, R. Yu, and B. Zhou, Cambridge University Press. In Press., 2021a.

700 IPCC: Summary for policymakers, in Climate Change 2021: The Physical Science Basis. Contribution of Working Group I to the Sixth Assessment Report of the Intergovernmental Panel on Climate Change, edited by V. Masson-Delmotte, P. Zhai, A. Pirani, S. L. Connors, C. Péan, S. Berger, N. Caud, Y. Chen, L. Goldfarb, M. I. Gomis, M. Huang, K. Leitzell, E. Lonnoy, J. B. R. Matthews, T. K. Maycock, T. Waterfield, O. Yelekçi, R. Yu, and B. Zhou, pp. 3–22, Cambridge University Press, Cambridge, United Kingdom and New York, NY, USA., 2021b.

705 ISONET Project Members, Schleser, G. H., Andreu-Hayles, L., Bednarz, Z., Berninger, F., Boettger, T., Dorado-Liñán, I., Esper, J., Grabner, M., Gutiérrez, E., Helle, G., Hilasvuori, E., Jugner, H., Kalela-Brundin, M., Krąpiec, M., Leuenberger, M., Loader, N. J., Masson-Delmotte, V., Pawełczyk, S., Pazdur, A., Pukienė, R., Rinne-Garmston, K. T., Saracino, A., Saurer, M., Sonninen, E., Stiévenard, M., Switsur, V. R. Szychowska-Krąpiec, E. Szczepanek, M., Todaro, L., Treydte, K., Vitas, A., Waterhouse, J. S., Weigl-Kuska, M. and Wimmer, R.: Stable oxygen isotope ratios of tree-ring cellulose from the site network of the EU-Project “ISONET,” GFZ Data Serv., doi:<https://doi.org/10.5880/GFZ.4.3.2023.001>, 2023.

715 Iturbide, M., Gutiérrez, J. M., Alves, L. M., Bedia, J., Cerezo-Mota, R., Gimeno, E., Cofiño, A. S., Luca, A. Di, Faria, S. H., Gorodetskaya, I. V., Hauser, M., Herrera, S., Hennessy, K., Hewitt, H. T., Jones, R. G., Krakovska, S., Manzanas, R., Martínez-Castro, D., Narisma, G. T., Nurhati, I. S., Pinto, I., Seneviratne, S. I., Hurk, B. van den and Vera, C. S.: An update of IPCC climate reference regions for subcontinental analysis of climate model data: definition and aggregated datasets, *Earth Syst. Sci. Data*, 12(4), doi:10.5194/essd-12-2959-2020, 2020.

720 Josse, J. and Husson, F.: missMDA: A Package for Handling Missing Values in Multivariate Data Analysis, *J. Stat. Softw.*, 70(1 SE-Articles), 1–31, doi:10.18637/jss.v070.i01, 2016.

Kahmen, A., Sachse, D., Arndt, S. K., Tu, K. P., Farrington, H., Vitousek, P. M. and Dawson, T. E.: Cellulose $\delta^{18}\text{O}$ is an index of leaf-to-air vapor pressure difference (VPD) in tropical plants, *Proc. Natl. Acad. Sci. U. S. A.*, 108(5), doi:10.1073/pnas.1018906108, 2011.

Labuhn, I., Daux, V., Pierre, M., Stievenard, M., Girardclos, O., Féron, A., Genty, D. and Masson-Delmotte, V., Mestre, O.:

- 725 Tree age, site and climate controls on tree ring cellulose $\delta^{18}\text{O}$: A case study on oak trees from south-western France, *Dendrochronologia*, 32, 78–89, doi:doi:10.1016/j.dendro.2013.11.001, 2014.
- Labuhn, I., Daux, V., Girardclos, O., Stievenard, M., Pierre, M. and Masson-Delmotte, V.: French summer droughts since 1326 CE: A reconstruction based on tree ring cellulose $\delta^{18}\text{O}$, *Clim. Past*, 12(5), 1101–1117, doi:doi:10.5194/cp-12-1101-2016, 2016.
- 730 Lawrence, M. G.: The relationship between relative humidity and the dewpoint temperature in moist air: A simple conversion and applications, *Bull. Am. Meteorol. Soc.*, 86(2), doi:10.1175/BAMS-86-2-225, 2005.
- Leonelli, G., Coppola, A., Salvatore, M. C., Baroni, C., Battipaglia, G., Gentilesca, T., Ripullone, F., Borghetti, M., Conte, E. and Tognetti, R.: Climate signals in a multispecies tree-ring network from central and southern Italy and reconstruction of the late summer temperatures since the early 1700s, *Clim. Past*, 13, 1451–1471, 2017.
- 735 Li, J., Wang, Z., Lai, C. and Zhang, Z.: Tree-ring-width based streamflow reconstruction based on the random forest algorithm for the source region of the Yangtze River, China, *Catena*, 183, doi:10.1016/j.catena.2019.104216, 2019.
- Lindgren, A., Lu, Z., Zhang, Q. and Hugelius, G.: Reconstructing Past Global Vegetation With Random Forest Machine Learning, Sacrificing the Dynamic Response for Robust Results, *J. Adv. Model. Earth Syst.*, 13(2), doi:10.1029/2020MS002200, 2021.
- 740 Liu, X., Zhang, X., Zhao, L., Xu, G., Wang, L., Sun, W., Zhang, Q., Wang, W., Zeng, X. and Wu, G.: Tree ring $\delta^{18}\text{O}$ reveals no long-term change of atmospheric water demand since 1800 in the northern Great Hinggan Mountains, China, *J. Geophys. Res. Atmos.*, 122, 6697–6712, 2017.
- Luterbacher, J., Dietrich, D., Xoplaki, E., Grosjean, M. and Wanner, H.: European Seasonal and Annual Temperature Variability, Trends, and Extremes since 1500, *Science (80-.)*, 303(5663), 1499–1503, doi:10.1126/science.1093877, 745 2004.
- Marengo, J. A., Nobre, C. A., Tomasella, J., Oyama, M. D., de Oliveira, G. S., de Oliveira, R., Camargo, H., Alves, L. M. and Brown, I. F.: The drought of Amazonia in 2005, *J. Clim.*, 21(3), doi:10.1175/2007JCLI1600.1, 2008.
- Marusek, J. A.: A Chronological Listing of Early Weather Events, *breadandbutter-science*, 580, 2010.
- Maxwell, A. E., Warner, T. A. and Fang, F.: Implementation of machine-learning classification in remote sensing: An applied 750 review, *Int. J. Remote Sens.*, 39(9), doi:10.1080/01431161.2018.1433343, 2018.
- McCarroll, D. and Loader, N. J.: Stable isotopes in tree rings, *Quat. Sci. Rev.*, 23(7–8), 771–801, doi:http://dx.doi.org/10.1016/j.quascirev.2003.06.017, 2004.
- McCarthy, G. D., Haigh, I. D., Hirschi, J. J.-M., Grist, J. P. and Smeed, D. A.: Ocean impact on decadal Atlantic climate variability revealed by sea-level observations, *Nature*, 521(7553), 508–510, doi:10.1038/nature14491, 2015.
- 755 Michel, S., Swingedouw, D., Chavent, M., Ortega, P., Mignot, J. and Khodri, M.: Reconstructing climatic modes of variability from proxy records using ClimIndRec version 1.0, *Geosci. Model Dev.*, 13(2), doi:10.5194/gmd-13-841-2020, 2020.
- Michel, S. L. L., Swingedouw, D., Ortega, P., Gastineau, G., Mignot, J., McCarthy, G. and Khodri, M.: Early warning signal for a tipping point suggested by a millennial Atlantic Multidecadal Variability reconstruction, *Nat. Commun.*, 13(1),

5176, doi:10.1038/s41467-022-32704-3, 2022.

- 760 Mohr, C. H., Manga, M., Helle, G., Heinrich, I., Giese, L. and Korup, O.: Trees Talk Tremor Wood Anatomy and Content
Reveal Contrasting Tree-Growth Responses to Earthquakes, *J. Geophys. Res. Biogeosciences*, 126, e2021JG006385,
doi:https://doi.org/10.1029/2021JG006385, 2021.
- Nagavciuc, V., Ionita, M., Perşoiu, A., Popa, I., Loader, N. J. and McCarroll, D.: Stable oxygen isotopes in Romanian oak tree
rings record summer droughts and associated large-scale circulation patterns over Europe, *Clim. Dyn.*, 52, 6557–6568,
765 doi:doi.org/10.1007/s00382-018-4530-7, 2019.
- Nagavciuc, V., Ionita, M., Kern, Z., McCarroll, D. and Popa, I.: A ~700 years perspective on the 21st century drying in the
eastern part of Europe based on $\delta^{18}O$ in tree ring cellulose, *Commun. Earth Environ.*, 3, 277, doi:10.1038/s43247-022-
00605-4, 2022.
- Nash, J. E. and Sutcliffe, J. V.: River flow forecasting through conceptual models part I - A discussion of principles, *J. Hydrol.*,
770 10(3), 282–290, doi:10.1016/0022-1694(70)90255-6, 1970.
- Novick, K. A., Ficklin, D. L., Stoy, P. C., Williams, C. A., Bohrer, G., Oishi, A. C., Papuga, S. A., Blanken, P. D., Noormets,
A., Sulman, B. N., Scott, R. L., Wang, L. and Phillips, R. P.: The increasing importance of atmospheric demand for
ecosystem water and carbon fluxes, *Nat. Clim. Chang.*, 6(11), doi:10.1038/nclimate3114, 2016.
- Ortega, P., Lehner, F., Swingedouw, D., Masson-Delmotte, V., Raible, C. C., Casado, M. and Yiou, P.: A model-tested North
775 Atlantic Oscillation reconstruction for the past millennium, *Nature*, 523(7558), 71–74, doi:10.1038/nature14518, 2015.
- Oshiro, T. M., Perez, P. S. and Baranauskas, J. A.: How many trees in a random forest?, in *Lecture Notes in Computer Science*
(including subseries *Lecture Notes in Artificial Intelligence* and *Lecture Notes in Bioinformatics*), vol. 7376 LNAI.,
2012.
- Pauling, A., Luterbacher, J., Casty, C. and Wanner, H.: Five hundred years of gridded high-resolution precipitation
780 reconstructions over Europe and the connection to large-scale circulation, *Clim. Dyn.*, 26(4), 387–405,
doi:10.1007/s00382-005-0090-8, 2006.
- Prasad, R., Ali, M., Kwan, P. and Khan, H.: Designing a multi-stage multivariate empirical mode decomposition coupled with
ant colony optimization and random forest model to forecast monthly solar radiation, *Appl. Energy*, 236,
doi:10.1016/j.apenergy.2018.12.034, 2019.
- 785 Qu, Y., Zhu, Z., Chai, L., Liu, S., Montzka, C., Liu, J., Yang, X., Lu, Z., Jin, R., Li, X., Guo, Z. and Zheng, J.: Rebuilding a
microwave soil moisture product using random forest adopting amsr-e/amsr2 brightness temperature and smap over the
Qinghai–Tibet Plateau, China, *Remote Sens.*, 11(6), doi:10.3390/rs11060683, 2019.
- Reichstein, M., Camps-Valls, G., Stevens, B., Jung, M., Denzler, J., Carvalhais, N. and Prabhat: Deep learning and process
understanding for data-driven Earth system science, *Nature*, 566(7743), doi:10.1038/s41586-019-0912-1, 2019.
- 790 Restaino, C. M., Peterson, D. L. and Littell, J.: Increased water deficit decreases Douglas fir growth throughout western US
forests, *Proc. Natl. Acad. Sci. U. S. A.*, 113(34), doi:10.1073/pnas.1602384113, 2016.
- Rinne, K. T., Loader, N. J., Switsur, V. R. and Waterhouse, J. S.: 400-year May - August precipitation reconstruction for

- Southern England using oxygen isotopes in tree rings, *Quat. Sci. Rev.*, 60, 13–25, doi:10.1016/j.quascirev.2012.10.048, 2013.
- 795 Roden, J., Lin, G. and Ehleringer, J. R.: A mechanistic model for interpretation of hydrogen and oxygen isotope ratios in tree-ring cellulose, *Geochim. Cosmochim. Acta*, 64(1), 21–35, 2000.
- Rodriguez-Galiano, V. F., Ghimire, B., Rogan, J., Chica-Olmo, M. and Rigol-Sanchez, J. P.: An assessment of the effectiveness of a random forest classifier for land-cover classification, *ISPRS J. Photogramm. Remote Sens.*, 67(1), doi:10.1016/j.isprsjprs.2011.11.002, 2012.
- 800 Roibu, C. C., Palaghianu, C., Nagavciuc, V., Ionita, M., Sfecla, V., Mursa, A., Crivellaro, A., Stirbu, M. I., Cotos, M. G., Popa, A., Sfecla, I. and Popa, I.: The Response of Beech (*Fagus sylvatica* L.) Populations to Climate in the Easternmost Sites of Its European Distribution, *Plants*, 11(23), doi:10.3390/plants11233310, 2022.
- Running, S. W.: Environmental control of leaf water conductance in conifers, *Can. J. For. Res.*, 6(1), doi:10.1139/x76-013, 1976.
- 805 Saurer, M., Borella, S., Schweingruber, F. and Siegwolf, R.: Stable carbon isotopes in tree rings of beech: Climatic versus site-related influences, *Trees - Struct. Funct.*, 11(5), doi:10.1007/s004680050087, 1997.
- Saurer, M., Cherubini, P., Reynolds-Henne, C. E., Treydte, K. S., Anderson, W. T. and Siegwolf, R. T. W.: An investigation of the common signal in tree ring stable isotope chronologies at temperate sites, *J. Geophys. Res. Biogeosciences*, 113 (G0403), 1–11, doi:10.1029/2008JG000689, 2008.
- 810 Saurer, M., Kress, A., Leuenberger, M., Rinne, K. T., Treydte, K. S. and Siegwolf, R. T. W.: Influence of atmospheric circulation patterns on the oxygen isotope ratio of tree rings in the Alpine region, *J. Geophys. Res. Atmos.*, 117(5), doi:10.1029/2011JD016861, 2012.
- Saurer, M., Spahni, R., Frank, D. C., Joos, F., Leuenberger, M., Loader, N. J., Mccarroll, D., Gagen, M., Poulter, B., Siegwolf, R. T. W., Andreu-Hayles, L., Boettger, T., Dorado Liñán, I., Fairchild, I. J., Friedrich, M., Gutierrez, E., Haupt, M., 815 Hilasvuori, E., Heinrich, I., Helle, G., Grudd, H., Jalkanen, R., Levanič, T., Linderholm, H. W., Robertson, I., Sonninen, E., Treydte, K., Waterhouse, J. S., Woodley, E. J., Wynn, P. M. and Young, G. H. F.: Spatial variability and temporal trends in water-use efficiency of European forests, *Glob. Chang. Biol.*, 20(12), doi:10.1111/gcb.12717, 2014.
- Seager, R., Hooks, A., Williams, A. P., Cook, B., Nakamura, J. and Henderson, N.: Climatology, variability, and trends in the U.S. Vapor pressure deficit, an important fire-related meteorological quantity, *J. Appl. Meteorol. Climatol.*, 54(6), 820 doi:10.1175/JAMC-D-14-0321.1, 2015.
- Siegwolf, R. T. W., Brooks, J. R., Roden, J. and Saurer, M.: *Stable Isotopes in Tree Rings Intrinsic Water-Use Efficiency Derived from Stable Carbon Isotopes of Tree-Rings*, Springer, Cham, Switzerland., 2022.
- Simmons, A. J., Willett, K. M., Jones, P. D., Thorne, P. W. and Dee, D. P.: Low-frequency variations in surface atmospheric humidity, temperature, and precipitation: Inferences from reanalyses and monthly gridded observational data sets, *J. 825 Geophys. Res. Atmos.*, 115(1), doi:10.1029/2009JD012442, 2010.
- Slivinski, L. C., Compo, G. P., Whitaker, J. S., Sardeshmukh, P. D., Giese, B. S., McColl, C., Allan, R., Yin, X., Vose, R.,

- Titchner, H., Kennedy, J., Spencer, L. J., Ashcroft, L., Brönnimann, S., Brunet, M., Camuffo, D., Cornes, R., Cram, T. A., Crouthamel, R., Domínguez-Castro, F., Freeman, J. E., Gergis, J., Hawkins, E., Jones, P. D., Jourdain, S., Kaplan, A., Kubota, H., Blancq, F. Le, Lee, T. C., Lorrey, A., Luterbacher, J., Maugeri, M., Mock, C. J., Moore, G. W. W. K. 830 K., Przybylak, R., Pudmenzky, C., Reason, C., Slonosky, V. C., Smith, C. A., Tinz, B., Trewin, B., Valente, M. A., Wang, X. L., Wilkinson, C., Wood, K. and Wyszyński, P.: Towards a more reliable historical reanalysis: Improvements for version 3 of the Twentieth Century Reanalysis system, *Q. J. R. Meteorol. Soc.*, 145(724), 2876–2908, doi:10.1002/qj.3598, 2019.
- Sternberg, L. and DeNiro, M. J.: Isotopic composition of cellulose from C3, C4, and CAM plants growing near one another, 835 *Science* (80-.), 220(4600), doi:10.1126/science.220.4600.947, 1983.
- Treydte, K., Schleser, G. H., Esper, J., Andreu, L., Bednarz, Z., Berninger, F., Böttger, T., D’Alessandro, C. D., Etien, N., Filot, M., Frank, D., Grabner, M., Gutierrez, E., Haupt, M., Helle, G., Hilasvuori, E., Jungner, H., Kalela-Brundin, M., Leuenberger, M., Loader, N., Masson-Delmotte, V., Pazdur, A., Planells, O., Pukiene, R., Reynolds, C., Rinne, K., Saurer, M., Sonninen, E., Stievenard, M., Switsur, R., Szczepanek, M., Todaro, L., Waterhouse, J., Weigl, M. and 840 Wimmer, R.: Climate signals in the European isotope network ISONET, *Tree rings Archaeol. Climatol. Ecol. TRACE*, 5, 138–147, 2007a.
- Treydte, K., Frank, D., Esper, J., Andreu, L., Bednarz, Z., Berninger, F., Boettger, T., D’Alessandro, C. M., Etien, N., Filot, M., Grabner, M., Guillemain, M. T., Gutierrez, E., Haupt, M., Helle, G., Hilasvuori, E., Jungner, H., Kalela-Brundin, M., Krapiec, M., Leuenberger, M., Loader, N. J., Masson-Delmotte, V., Pazdur, A., Pawelczyk, S., Pierre, M., Planells, 845 O., Pukiene, R., Reynolds-Henne, C. E., Rinne, K. T., Saracino, A., Saurer, M., Sonninen, E., Stievenard, M., Switsur, V. R., Szczepanek, M., Szychowska-Krapiec, E., Todaro, L., Waterhouse, J. S., Weigl, M. and Schleser, G. H.: Signal strength and climate calibration of a European tree-ring isotope network, *Geophys. Res. Lett.*, 34, L24302(24), 1–6, doi:10.1029/2007GL031106, 2007b.
- Trigo, R. M., Vaquero, J. M., Alcoforado, M. J., Barriendos, M., Taborda, J., García-Herrera, R. and Luterbacher, J.: Iberia in 850 1816, the year without a summer, *Int. J. Climatol.*, 29(1), doi:10.1002/joc.1693, 2009.
- Tyralis, H., Papacharalampous, G. and Langousis, A.: A brief review of random forests for water scientists and practitioners and their recent history in water resources, *Water (Switzerland)*, 11(5), doi:10.3390/w11050910, 2019.
- Vitas, A.: Tree-ring chronology of Scots pine (*Pinus sylvestris* L.) for Lithuania, *Balt. For.*, 14(2), 2008.
- Wang, J., Yang, B., Ljungqvist, F. C., Luterbacher, J., Osborn, T. J., Briffa, K. R. and Zorita, E.: Internal and external forcing 855 of multidecadal Atlantic climate variability over the past 1,200 years, *Nat. Geosci.*, 10(7), 512–517, doi:10.1038/ngeo2962, 2017.
- Willett, K. M., Dunn, R. J. H., Thorne, P. W., Bell, S., De Podesta, M., Parker, D. E., Jones, P. D. and Williams, C. N.: HadISDH land surface multi-variable humidity and temperature record for climate monitoring, *Clim. Past*, 10(6), doi:10.5194/cp-10-1983-2014, 2014.
- 860 Williams, A. P., Allen, C. D., Macalady, A. K., Griffin, D., Woodhouse, C. A., Meko, D. M., Swetnam, T. W., Rauscher, S.

- A., Seager, R., Grissino-Mayer, H. D., Dean, J. S., Cook, E. R., Gangodagamage, C., Cai, M. and Mcdowell, N. G.: Temperature as a potent driver of regional forest drought stress and tree mortality, *Nat. Clim. Chang.*, 3(3), doi:10.1038/nclimate1693, 2013.
- 865 WMO: Technical Regulations Basic Documents No. 2 Volume II – Meteorological Service for International Air Navigation, WMO-No. 49, , 206 [online] Available from: <https://library.wmo.int/records/item/35795-technical-regulations-volume-ii-meteorological-service-for-international-air-navigation>, 2018.
- Yang, J., Jiang, L., Luo, K., Pan, J., Lemmetyinen, J., Takala, M. and Wu, S.: Snow depth estimation and historical data reconstruction over China based on a random forest machine learning approach, *Cryosphere*, 14(6), doi:10.5194/tc-14-1763-2020, 2020.
- 870 Yuan, W., Zheng, Y., Piao, S., Ciais, P., Lombardozzi, D., Wang, Y., Ryu, Y., Chen, G., Dong, W., Hu, Z., Jain, A. K., Jiang, C., Kato, E., Li, S., Lienert, S., Liu, S., Nabel, J. E. M. S., Qin, Z., Quine, T., Sitch, S., Smith, W. K., Wang, F., Wu, C., Xiao, Z. and Yang, S.: Increased atmospheric vapor pressure deficit reduces global vegetation growth, *Sci. Adv.*, 5(8), doi:10.1126/sciadv.aax1396, 2019.
- 875 Zhan, Y., Luo, Y., Deng, X., Grieneisen, M. L., Zhang, M. and Di, B.: Spatiotemporal prediction of daily ambient ozone levels across China using random forest for human exposure assessment, *Environ. Pollut.*, 233, doi:10.1016/j.envpol.2017.10.029, 2018.
- Zhang, Q., Ficklin, D. L., Manzoni, S., Wang, L., Way, D., Phillips, R. P. and Novick, K. A.: Response of ecosystem intrinsic water use efficiency and gross primary productivity to rising vapor pressure deficit, *Environ. Res. Lett.*, 14, 074023, doi:10.1088/1748-9326/ab2603, 2019.
- 880 Zhao, C., Liu, B., Piao, S., Wang, X., Lobell, D. B., Huang, Y., Huang, M., Yao, Y., Bassu, S., Ciais, P., Durand, J. L., Elliott, J., Ewert, F., Janssens, I. A., Li, T., Lin, E., Liu, Q., Martre, P., Müller, C., Peng, S., Peñuelas, J., Ruane, A. C., Wallach, D., Wang, T., Wu, D., Liu, Z., Zhu, Y., Zhu, Z. and Asseng, S.: Temperature increase reduces global yields of major crops in four independent estimates, *Proc. Natl. Acad. Sci. U. S. A.*, 114(35), doi:10.1073/pnas.1701762114, 2017.